Cell Reports

Article

High FOXA1 levels induce ER transcriptional reprogramming, a pro-metastatic secretome, and metastasis in endocrine-resistant breast cancer

Graphical abstract

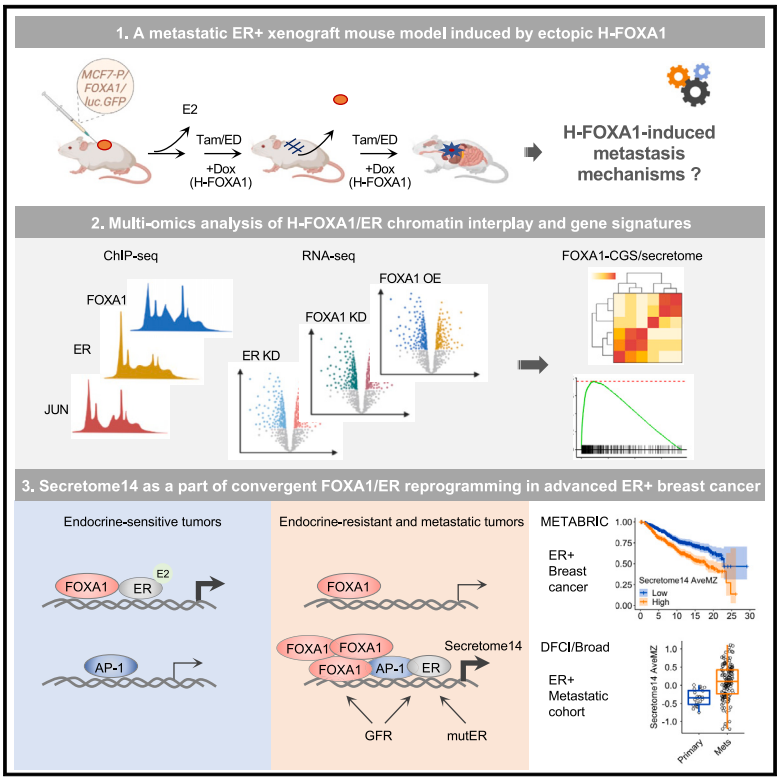

Highlights

- High FOXA1 promotes tamoxifen-treated xenograft tumor metastasis in mice
- High FOXA1 induces a core gene signature in ER+ breast cancer endocrine resistance
- Secretome14, as a high FOXA1/ER target, predicts poor outcomes of ER+ breast cancer
- A convergent pathway activating Secretome14 underpins ER+ tumor metastasis

Authors

Xiaoyong Fu, Resel Pereira, Chia-Chia Liu, ..., Mothaffar F. Rimawi, C. Kent Osborne, Rachel Schiff

Correspondence

xiaoyonf@wecurecancer.org (X.F.), rschiff@bcm.edu (R.S.)

In brief

Fu et al. show that ectopic high FOXA1 promotes ER+ breast cancer metastasis in a xenograft mouse model. Integrated omics data analysis identifies Secretome14 as a high FOXA1/ER target of convergent signaling, including high growth factor receptor signaling. Secretome14 is a strong predictor of poor outcomes of ER+ breast cancer.

Fu et al., 2023, Cell Reports *42*, 112821
August 29, 2023
https://doi.org/10.1016/j.celrep.2023.112821

CellPress

Cell Reports

CellPress
OPEN ACCESS

Article

High FOXA1 levels induce ER transcriptional reprogramming, a pro-metastatic secretome, and metastasis in endocrine-resistant breast cancer

Xiaoyong Fu,[1,2,3,15,17,*] Resel Pereira,[1,2,3] Chia-Chia Liu,[1,2,4] Carmine De Angelis,[1,2,4,5] Martin J. Shea,[1,2,4] Sarmistha Nanda,[1,2,4] Lanfang Qin,[1,2,4] Tamika Mitchell,[1,2,4,16] Maria L. Cataldo,[1,2,4,5] Jamunarani Veeraraghavan,[1,2,4] Vidyalakshmi Sethunath,[1,2,4] Mario Giuliano,[1,5] Carolina Gutierrez,[6] Balázs Győrffy,[7,8] Meghana V. Trivedi,[1,2,4,9,10] Ofir Cohen,[11,12,13] Nikhil Wagle,[11,12] Agostina Nardone,[11,14] Rinath Jeselsohn,[11,14] Mothaffar F. Rimawi,[1,2,4] C. Kent Osborne,[1,2,3,4] and Rachel Schiff[1,2,3,4,*]

[1]Lester and Sue Smith Breast Center, Baylor College of Medicine, Houston, TX 77030, USA
[2]Dan L. Duncan Comprehensive Cancer Center, Baylor College of Medicine, Houston, TX 77030, USA
[3]Department of Molecular and Cellular Biology, Baylor College of Medicine, Houston, TX 77030, USA
[4]Department of Medicine, Baylor College of Medicine, Houston, TX 77030, USA
[5]Department of Clinical Medicine and Surgery, University of Naples Federico II, Naples, Italy
[6]Department of Pathology, Baylor College of Medicine, Houston, TX 77030, USA
[7]Department of Bioinformatics, Semmelweis University, 1085 Budapest, Hungary
[8]RCNS Cancer Biomarker Research Group, Institute of Enzymology, Magyar Tudósok körútja 2, 1117 Budapest, Hungary
[9]Department of Pharmacy Practice and Translational Research, University of Houston, Houston, TX 77204, USA
[10]Department of Pharmacological and Pharmaceutical Sciences, University of Houston, Houston, TX 77204, USA
[11]Department of Medical Oncology, Dana-Farber Cancer Institute, Harvard Medical School, Boston, MA 02210, USA
[12]Broad Institute of MIT and Harvard, Cambridge, MA 02142, USA
[13]Department of Microbiology, Immunology, and Genetics, Faculty of Health Sciences, Ben-Gurion University, Beer-Sheva 84105, Israel
[14]Center for Functional Cancer Epigenetics, Dana-Farber Cancer Institute, Harvard Medical School, Boston, MA 02210, USA
[15]Present address: Gilead Sciences Inc., 333 Lakeside Dr., Foster City, CA 94404, USA
[16]Deceased
[17]Lead contact
*Correspondence: xiaoyonf@wecurecancer.org (X.F.), rschiff@bcm.edu (R.S.)
https://doi.org/10.1016/j.celrep.2023.112821

SUMMARY

Aberrant activation of the forkhead protein FOXA1 is observed in advanced hormone-related cancers. However, the key mediators of high FOXA1 signaling remain elusive. We demonstrate that ectopic high FOXA1 (H-FOXA1) expression promotes estrogen receptor-positive (ER+) breast cancer (BC) metastasis in a xenograft mouse model. Mechanistically, H-FOXA1 reprograms ER-chromatin binding to elicit a core gene signature (CGS) enriched in ER+ endocrine-resistant (EndoR) cells. We identify Secretome14, a CGS subset encoding ER-dependent cancer secretory proteins, as a strong predictor for poor outcomes of ER+ BC. It is elevated in ER+ metastases vs. primary tumors, irrespective of *ESR1* mutations. Genomic ER binding near Secretome14 genes is also increased in mutant ER-expressing or mitogen-treated ER+ BC cells and in ER+ metastatic vs. primary tumors, suggesting a convergent pathway including high growth factor receptor signaling in activating pro-metastatic secretome genes. Our findings uncover H-FOXA1-induced ER reprogramming that drives EndoR and metastasis partly via an H-FOXA1/ER-dependent secretome.

INTRODUCTION

Estrogen receptor (ER) is a key transcription factor (TF) regulating expression of genes in normal mammary gland development and ER-positive (ER+) breast cancer (BC).[1,2] Endocrine therapy is the mainstay treatment of ER+ BC, including selective ER modulators (SERMs; i.e., tamoxifen), aromatase inhibitors (AIs) that block synthesis of estrogen, and selective ER degraders (SERDs; i.e., fulvestrant). However, endocrine resistance (EndoR) is common, resulting in disease progression and poor clinical outcome.[3,4]

In the majority of EndoR tumors, ER continues to exert a pivotal, albeit altered, role in driving ER+ BC progression.[5] Main contributing causes of EndoR are estrogen-independent and modulated SERM/SERD effects on ER activation, which can stem from (1) increased ER-coactivator interactions,[6–8] (2) cross-talk between ER and high growth factor receptor (GFR) signaling,[9,10] and/or (3) the recently identified *ESR1*

ligand-independent activating mutations in over 30% of metastatic BC, particularly in patients treated with AIs.[11]

Genome-wide mapping of TF-chromatin binding (cistrome) reveals a dynamic pattern of ER redistribution in EndoR cell models and ER+ metastatic tumors, in which the genes harboring newly established ER binding sites predict poor prognosis of ER+ BC.[12–15] One key factor regulating ER-chromatin binding is the forkhead box protein FOXA1,[16,17] a pioneer TF functioning at the epigenetic level by facilitating chromatin decondensation and subsequent lineage-specific TF binding and gene activation.[18,19] We and others have shown that high levels of FOXA1 (H-FOXA1), via genetic amplification, activating mutations, or local structural alterations, and/or overexpression, occur in preclinical EndoR cell models[20] and in hormone receptor-driven metastatic breast and/or prostate cancers.[21–25] Notably, the pioneering activity of FOXA1 may also differ based on its expression levels and on hormonal signals because it has been shown that, whereas FOXA1 binding to chromatin occurs prior to ER recruitment,[26] ER may also facilitate a small group of FOXA1 binding upon estrogen stimulation.[27,28] However, the functional consequences of H-FOXA1 in EndoR and metastatic BC remain to be addressed.

In this report, we first tested the hypothesis that H-FOXA1 promotes EndoR BC metastasis by employing a doxycycline (Dox)-inducible FOXA1 overexpression (OE) xenograft mouse model. This syngeneic H-FOXA1 cell model allowed us to delineate the direct effect of H-FOXA1 on the ER cistrome aligned with the FOXA1/ER-dependent transcriptome without superimposition of other potential genetic alterations arising upon acquired resistance. We then performed integrated omics data analyses to characterize H-FOXA1/ER signaling in EndoR BC cells. We show that H-FOXA1 promotes tamoxifen-resistant (TamR) BC xenograft tumor metastasis and induces a core gene signature (CGS) enriched in ER+ EndoR BC cell models. We further demonstrate that Secretome14, encoding a highly select H-FOXA1/ER-dependent secretome subset, predicts poor outcomes of ER+ BC. Secretome14 expression escalates in ER+ metastases and harbors increased ER binding at *cis*-regulatory regions in ER+ cell models expressing mutant ER or treated with mitogens and in ER+ metastases compared with the respective primary tumors.

Our findings support the role of H-FOXA1 in promoting Tam-treated BC metastasis and reveal the H-FOXA1/ER-dependent Secretome14 as a part of convergent ER reprogramming in advanced ER+ disease progression.

RESULTS

Ectopic FOXA1 OE in a xenograft mouse model promotes TamR tumor metastasis

Because FOXA1 upregulation occurs frequently in ER+ metastatic BC,[21,22] we tested the hypothesis that H-FOXA1 drives EndoR and metastasis *in vivo*. We generated an orthotopic xenograft mouse model by injection of luciferase/GFP-tagged MCF7 cells engineered with Dox-inducible FOXA1 OE. We randomized mice bearing estrogen (E2)-stimulated tumors to ± Dox groups treated with Tam in the absence of E2, with estrogen deprivation (ED) alone, or continuing E2 as a control (Figure 1A, left panel). Primary xenograft tumors, when reaching a volume greater than 600 mm^3, were surgically removed, followed by periodic bioluminescence imaging (BLI) to monitor tumor metastasis (Figure 1A, right panel). All primary tumors treated with E2 continued to grow, with no difference in progression-free survival (PFS) between the −Dox and +Dox groups (Figures S1A–S1C). Tam and ED led to initial tumor regression, followed by tumor recurrence, which was faster with larger tumor size in the Tam vs. ED group (Figures S1D–S1G; Table S1). Of note, a few tumors progressed earlier in the Tam +Dox vs. −Dox group, but overall, for the Tam and ED groups, FOXA1 OE did not result in a significant difference in PFS or regression-free survival over an extended time (Figures S1H and S1I; Table S1). Importantly, after survival surgery, we observed an increased rate of axillary lymph node (LN) metastasis in the Tam +Dox vs. −Dox group (Figures 1B and 1C). The BLI signal in isolated lungs after euthanasia was also significantly enhanced in the Tam +Dox vs. −Dox group (Figure 1D). Overall, there was an inferior LN/distant relapse-free survival (DRFS) in mice treated with Tam +Dox vs. −Dox, with a median time of 60 days for metastatic onset in the +Dox group (Figure 1E; Table S1). Compared with Tam, fewer mice received survival surgery in the ED group, with no difference in RFS between the ED + Dox vs. −Dox group (Figures S1J and S1K). Overall, these data suggest that, despite no change in primary tumor endocrine response, ectopic FOXA1 OE promotes metastasis in xenograft tumors treated with Tam but not ED.

All metastatic LN lesions were confirmed by necroscopic BLI and further identified as of MCF7 origin by GFP immunohistochemistry (IHC) (Figures S2A and 1F; Table S1). FOXA1 expression was comparable in E2-treated tumors with ectopic FOXA1 OE and the acquired TamR tumors, in which +Dox further increased FOXA1 levels (Figures S2B–S2D). ER expression was maintained, whereas the classic ER-regulated target progesterone receptor (PR) was lost in TamR vs. E2-treated xenograft tumors (Figures S2C and S2E). FOXA1 OE in resistant tumors was functionally relevant because the H-FOXA1 target interleukin-8 (IL-8)[20] was further upregulated in +Dox vs. −Dox TamR tumors (Figures S2C and S2F). Similar data showing FOXA1 expression and PR loss were also seen in the resistant cell model *in vitro* (Figure S2G). Of note, ectopic FOXA1 OE led to a reduction of PR expression in MCF7-parental (P) cells (Figure S2G) but not in E2-treated MCF7-P xenograft tumors (Figure S2B), possibly because of the effect of exogenous E2 supplementation on *in vivo* xenograft tumors. Indeed, E2 treatment in MCF7-P cells with ectopic FOXA1 OE partly negated, in a dose-dependent manner, the reduction in PR (Figure S2H), suggesting regained classic ER activity upon E2 even in the presence of H-FOXA1.

H-FOXA1 coordinates ER to reprogram genome-wide ER and FOXA1 binding in endocrine-naive cells

To dissect the interplay between H-FOXA1 and ER in cistromic and transcriptomic reprogramming, we integrated the FOXA1 and ER cistrome in endocrine-naive cells with ectopic FOXA1 OE and in the *FOXA1*-amplified TamR cells with endogenous H-FOXA1. We first mapped the ER cistrome by chromatin immunoprecipitation followed by next-generation sequencing

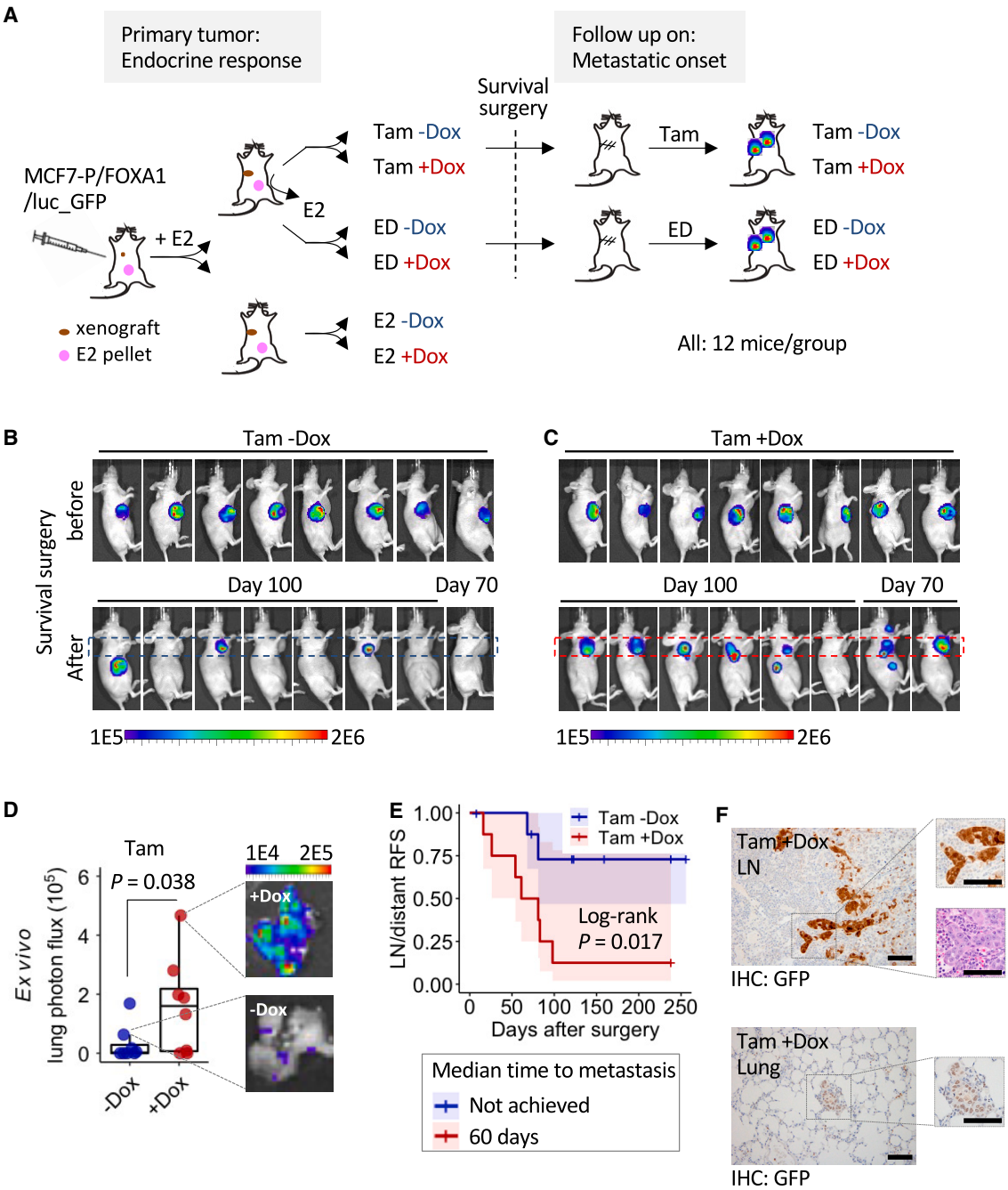

Figure 1. Ectopic FOXA1 overexpression (OE) promotes Tam-treated xenograft tumor metastasis

(A) Schematic of the *in vivo* experiments to assess the impact of ectopic FOXA1 OE on primary tumor endocrine response (left) and metastatic onset after survival surgery (right).

(B and C) Live bioluminescence imaging (BLI) shows primary tumor and axillary lymph node (LN) metastases (mets) post survival surgery in Tam ± Dox groups. Dashed rectangles mark the armpit regions with LN mets. Scaled color bars denote the pixel value of photon flux.

(D) Quantification of BLI signal in lungs harvested from euthanized mice in the Tam ± Dox groups. The p value was determined by Wilcoxon rank-sum test. Scaled color bars denote the pixel value of photon flux.

(E) Kaplan-Meier plots depicting LN/distant relapse-free survival (DRFS) measured by counting events of the first observed metastatic onset after survival surgery. The p value was determined using the log rank survival test. Bottom: the calculated median time to metastasis of the Tam ± Dox groups.

(F) Representative GFP immunohistochemistry (IHC) staining on LNs and lungs harvested from the Tam +Dox group. Scale bars, 100 μm.

See also Figures S1 and S2.

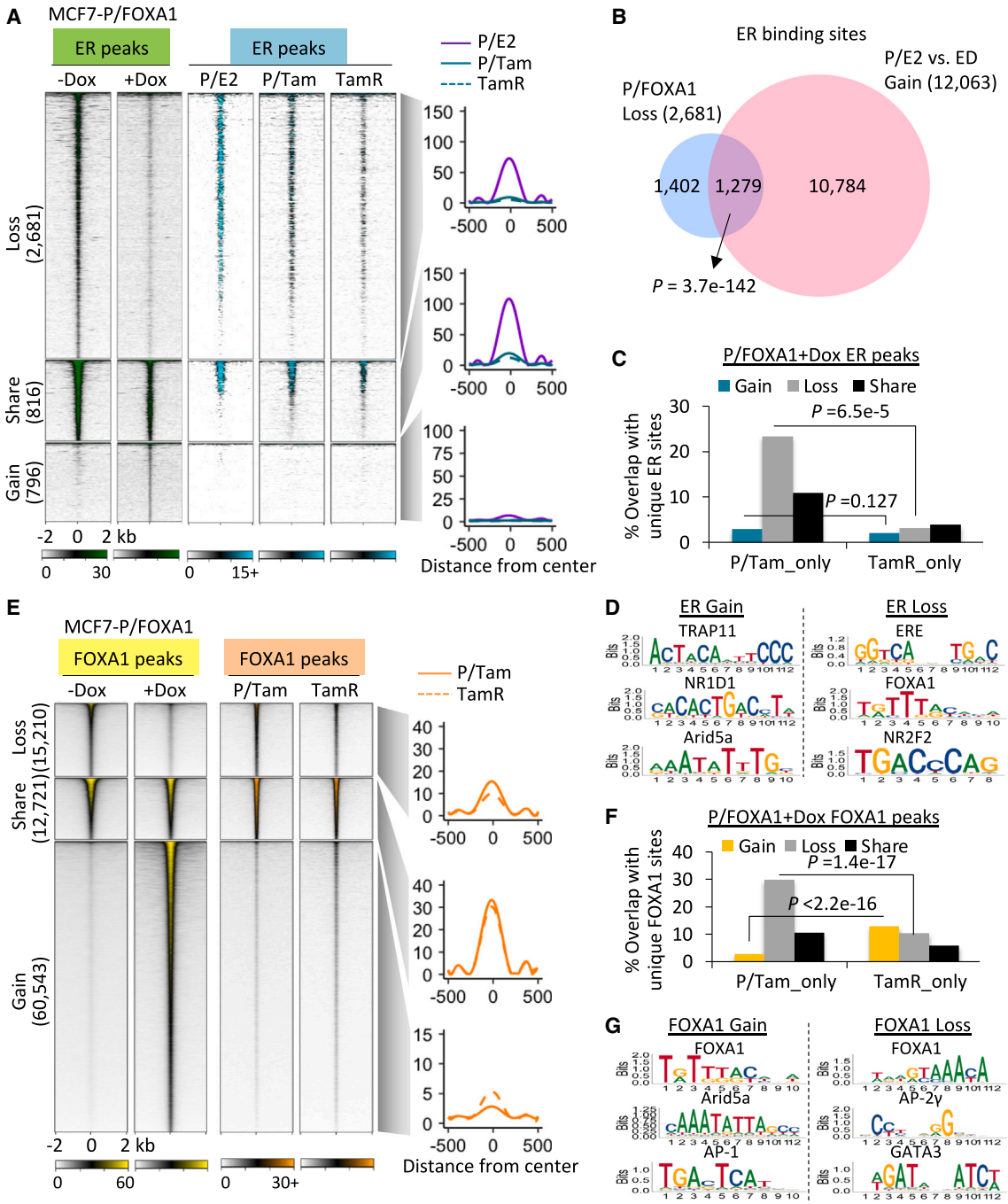

Figure 2. Ectopic FOXA1 OE reprograms genome-wide ER and FOXA1 binding

(A) Heatmaps showing the intensity of the ER-bound peaks in MCF7-P/FOXA1 +Dox vs. −Dox cells. Also shown is the intensity of overlaid regions bound by ER in E2- or Tam-treated P cells and in TamR cells. Right: the average intensity of the overlaid ER binding.

(B) Venn diagram showing the overlap of ER binding sites between the H-FOXA1-induced ER loss regions and the ER gain regions in P cells upon E2 stimulation. The p value was determined using the Pearson's chi-squared test with Yates' continuity correction.

(C) Bar charts depicting the proportion of the clustered ER binding sites in P/FOXA1 +Dox vs. −Dox cells that overlap with the unique ER binding sites in Tam-treated P and TamR cells.

(D) Top enriched binding motifs at the ER gain and loss regions in P/FOXA1 +Dox vs. −Dox cells.

(E) Heatmaps showing the intensity of the FOXA1-bound peaks in MCF7-P/FOXA1 +Dox vs. −Dox cells. Also shown is the intensity of overlaid regions bound by FOXA1 in Tam-treated P and TamR cells. Right: the average intensity of the overlaid FOXA1 binding.

(legend continued on next page)

(ChIP-seq). As shown in Figure 2A, even without endocrine therapy, H-FOXA1 altered the ER cistrome, resulting in redistribution of more than 80% of ER with 2,681 decreased and 796 increased binding events in +Dox vs. −Dox cells. Importantly, compared with FOXA1 OE, ectopic yellow fluorescent protein (YFP) expression as a control led to an indiscernible change in the ER cistrome in MCF7-P cells (Figures S3A–S3C). The difference in H-FOXA1-induced loss/gain of ER binding was not seen in P cells upon YFP expression, ruling out an effect of Dox on altering ER binding events (Figures S3D and S3E). To determine whether the H-FOXA1-dependent ER cistrome is related to the ER cistrome in acquired TamR cells harboring *FOXA1* amplification, we overlaid the differential ER binding with our prior ER ChIP-seq data obtained from MCF7-P and TamR cells.[12] We found that the majority of lost or retained ER binding induced by ectopic H-FOXA1 overlapped with the ER binding sites in P cells induced by E2 vs. Tam treatment (Figure 2A, right panel). The lost ER binding sites induced by H-FOXA1 in P cells were also significantly enriched for ER binding under E2 vs. ED, which corresponds to 11% of total E2-stimulated ER binding (Figure 2B), suggesting that H-FOXA1 induces loss of selective E2-stimulated ER binding sites. We further found that the proportion of H-FOXA1-induced ER loss regions was significantly enriched for the unique ER binding sites in P vs. TamR cells, but no enrichment of the ER gain regions was observed in the unique ER binding in TamR vs. P cells (Figure 2C). This possibly reflects a discrepancy in ER reprogramming, especially for the gain regions, under H-FOXA1 induced by transient (+Dox) vs. the long-term process of acquired resistance as well as regular vs. estrogen-deprived medium in P vs. TamR cells, respectively. Motif analysis revealed the canonical estrogen response element (ERE) as the top motif enriched in the ER loss regions induced by H-FOXA1 (Figure 2D; Table S2), further supporting the notion that H-FOXA1 reduces genome-wide ER binding at regions that are normally enriched for selective E2-stimulated binding sites. Notably, by overlaying the FOXA1 cistrome[29] over the ER cistrome in the same P cells with ectopic H-FOXA1 induction, we observed parallel reduced or enhanced FOXA1 binding at the lost/shared and a subset of gained ER binding sites, respectively (Figure S3F). Altogether, our findings suggest direct involvement of FOXA1 in ER cistromic redistribution, possibly via mechanisms including recruitment of co-activators/co-repressors and FOXA1-engaged chromatin remodeling, as shown by previous studies.[26,29–31]

We have shown previously that ectopic H-FOXA1 induces enhancer reprogramming in endocrine-sensitive BC cells.[29] To compare the H-FOXA1 cistrome with the one established upon acquired resistance, we now integrated differential FOXA1 binding sites identified in the inducible FOXA1 OE cell model[29] with the FOXA1 cistrome mapped in MCF7-P and TamR cells expressing endogenous H-FOXA1 because of acquired *FOXA1* amplification.[20] We observed a concordant decrease, sharing, and increase in FOXA1 binding in TamR vs. P cells at the corresponding differential FOXA1-bound regions in P cells with inducible FOXA1 OE (Figure 2E). This is consistent with a significant enrichment of H-FOXA1-induced FOXA1 gain (13%) and FOXA1 loss (30%) regions at the unique FOXA1 binding sites in TamR or P cells, respectively (Figure 2F). In the H-FOXA1-induced ER gain and H-FOXA1-induced FOXA1 gain regions, we found the enriched ARID5A motif (Figures 2D and 2G; Table S2). Of note, ARID1A, a member of the AT-rich interactive domain (ARID) protein family and a subunit of the SWI/SNF chromatin remodeling complex, has been shown recently to maintain FOXA1/ER-dependent luminal lineage-determining gene expression, and its inactivating mutations alter gene expression programs, resulting in EndoR in advanced ER+ BC.[30,31]

Collectively, our data suggest that ectopic FOXA1 OE in endocrine-naive P cells reprograms the ER and FOXA1 cistrome similarly as those established in TamR cells expressing H-FOXA1 via *FOXA1* amplification.

Ectopic FOXA1 OE induces a shared CGS across different H-FOXA1 cell models

Genomic binding of FOXA1 at the canonical forkhead motif could be saturated by ectopic H-FOXA1, which may cause an artifact when analyzing H-FOXA1 biological outcomes. Interestingly, by scanning the FOXA1 motif across the genome-wide enhancer regions in the MCF7-P/FOXA1 cell model, we found that only 23.7% of the FOXA1 motifs across the genome were bound by FOXA1 in −Dox and/or +Dox cells (Figure 3A). These FOXA1-bound FOXA1 motif sites also exhibit differential FOXA1 binding affinity in +Dox vs. −Dox cells (Figure 3B). These findings exclude the possibility of FOXA1 saturation and support the notion that pioneer factors like FOXA1 exhibit select and specific genomic binding even when expressed ectopically.[32]

To link gene expression to the FOXA1-bound sites that harbor the FOXA1 motif, we identified all genes harboring nearby FOXA1 motifs with FOXA1 occupation in MCF7-P/FOXA1 ± Dox cells. We observed a strong correlation between the number of gained FOXA1-bound motifs and the degree of gene expression upregulation by ectopic FOXA1 OE (Figure 3C). Next, using the binding and expression target analysis (BETA) algorithm,[33] we identified 471 upregulated (UP) and 311 downregulated (DN) genes in +Dox vs. −Dox cells (Table S2), which we defined as the H-FOXA1-induced CGS (Figure 3D). This FOXA1-CGS was highly enriched in the altered transcriptomes of two additional ER+ BC cell models (ZR75-1 and T47D) expressing ectopic Dox-induced H-FOXA1 (Figures 3E, 3F, S4A, and S4B). Moreover, the CGS_UP gene set was also enriched in pancreatic and prostate cancer cells with ectopic H-FOXA1 OE[34,35] (Figures S4C and S4D), suggesting a similar impact of H-FOXA1 on the transcriptome in a diverse epithelial cancer cell context.

Functional annotation of the FOXA1-CGS showed an enrichment of the Gene Ontology (GO) terms[36] "cell-cell adhesion mediated by integrin," "TGF beta receptor signaling pathway,"

(F) Bar charts showing the proportion of the clustered FOXA1 binding sites in P/FOXA1 +Dox vs. −Dox cells that overlap with the unique FOXA1 binding sites in Tam-treated P and TamR cells.

(G) Top enriched binding motifs at the FOXA1 gain and loss regions in P/FOXA1 +Dox vs. −Dox cells.

For (C) and (F), the p value was determined using a chi-square test with Bonferroni multicomparison adjustment. See also Figure S3.

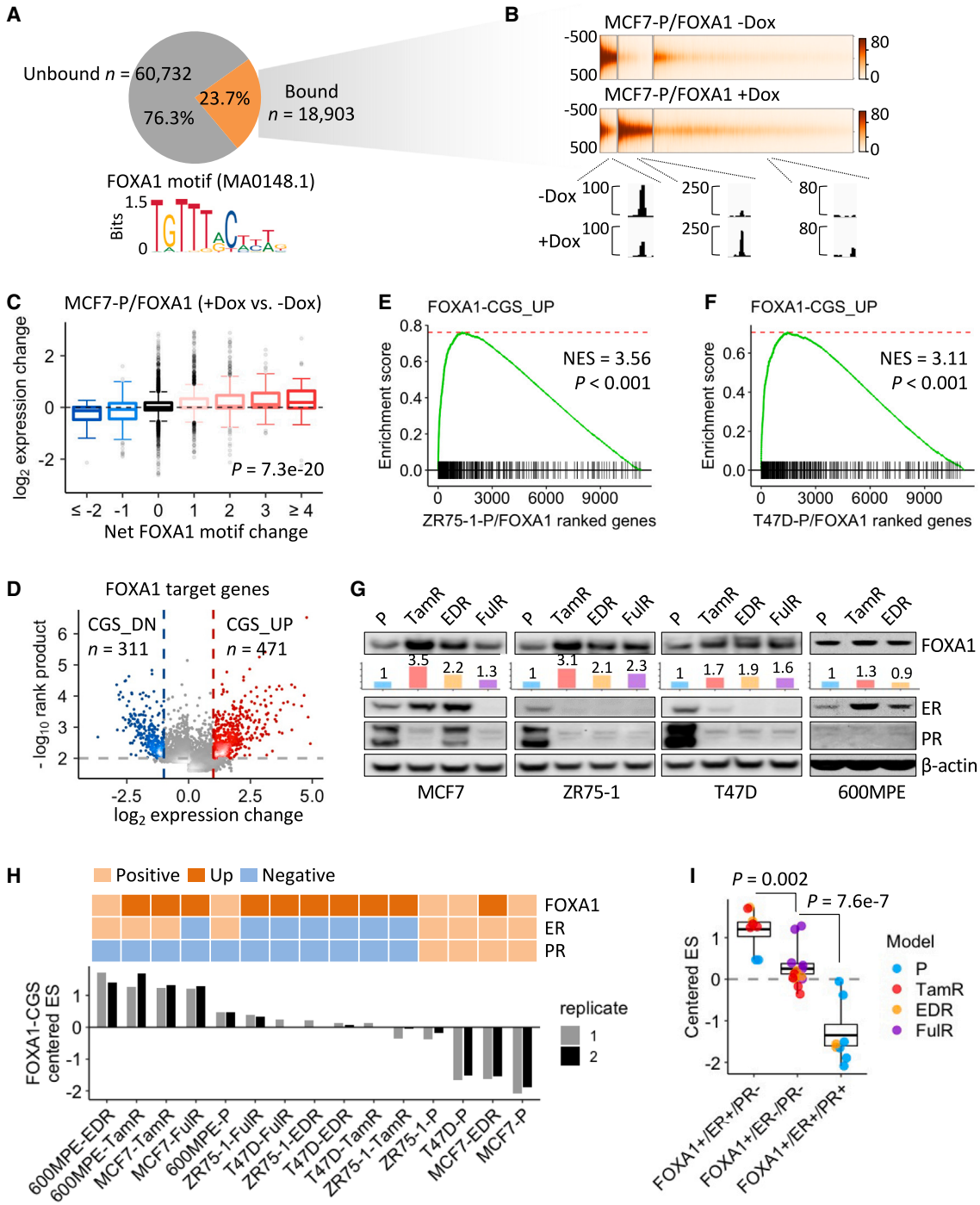

Figure 3. H-FOXA1 induces a core gene signature (CGS) that distinguishes ER+ EndoR BC cells

(A) Pie chart displaying the proportion of the FOXA1-bound motif in MCF7-P/FOXA1 ± Dox cells among the reservoir of the genome-wide scanned FOXA1 motif (JASPAR: MA0148.1). The motif sequence logo is shown in the bottom panel.

(B) Heatmaps showing the intensity of the FOXA1-bound peaks at the FIMO-scanned FOXA1 motif in P/FOXA1 +Dox vs. −Dox cells. Representative peaks shown by the genome browser tracks are included in the bottom panel.

(C) Boxplots showing correlation between the counted FOXA1 motif and the expression of nearby genes in MCF7-P/FOXA1 +Dox vs. −Dox cells. The p value was determined using one-way ANOVA.

(D) Volcano plot depicting the expression changes (x axis) and the probability of H-FOXA1 targets (y axis) predicted by the BETA algorithm.[33] FOXA1-CGS_downregulated (DN) and upregulated (UP) genes are colored in blue and red, respectively, based on the cutoff, as indicated by the dashed lines.

(legend continued on next page)

and "extracellular matrix disassembly" for the CGS_UP gene set (Figure S4E) and "amino acid transport," "tRNA aminoacylation for protein translation," and "response to estrogen" for the CGS_DN gene set (Figure S4F). Gene set enrichment analysis (GSEA) further confirmed the top enrichment of the FOXA1-CGS in the three H-FOXA1 ER+ BC cell models (Figures S5A–S5C). In addition, the enriched Molecular Signatures Database (MSigDB) hallmark gene sets,[37] shared by the three H-FOXA1 cell models (Table S2), include "inflammatory response," "complement," and "interferon gamma response" for H-FOXA1-induced (Figure S5D) and "estrogen response early" and "estrogen response late" for H-FOXA1-repressed genes (Figure S5E). These findings support an H-FOXA1 induced immune-related signature over that of an estrogen-responding signature.

The FOXA1-CGS is highly represented in ER+ EndoR BC cell models

To further evaluate and generalize the relevance of the FOXA1-CGS in EndoR, we queried the RNA sequencing (RNA-seq) data obtained from four ER+ BC cell models with their EndoR derivatives made resistant to Tam, ED (EDR), or fulvestrant (FulR).[20,38] FOXA1 levels were elevated in EndoR derivatives of the MCF7, ZR75-1, and T47D models, whereas ER expression, as we have shown previously,[38] was largely lost upon EndoR in the latter two models (Figure 3G). Expression of PR, the classical E2-stimulated ER target, was lost in all resistant derivatives except for the MCF7-EDR model, in which classic E2-dependent ER activity is maintained.[38,39] Indeed, hierarchical clustering of the FOXA1-CGS genes separated the group of EDR, P (grown in full medium), and E2-treated P cells (grown in ED medium) from the TamR and FulR derivatives (Figures S5F and S5G). We then sorted all P and EndoR models using the FOXA1-CGS enrichment score calculated by single-sample (ss) GSEA[40] (Figure 3H) and saw decreasing FOXA1-CGS scores in these models in the order ER+/PR− > ER−/PR− > ER+/PR+ (Figure 3I), further uncovering a potential clinical relevance.

The FOXA1-CGS is enriched for an H-FOXA1/ER-dependent secretome in ER+ EndoR cells

We found that H-FOXA1 induces a transcriptome enriched for immune response signaling (Figure S5D), which is consistent with the notion that H-FOXA1 induces IL-8 in TamR vs. P cells, as we described previously.[20] Here we performed an unbiased proteomics analysis using a cell proteome database[41] and found a significant enrichment of secretory proteins encoded by the FOXA1-CGS compared with genes not altered by H-FOXA1 (Figure 4A). This enrichment was also confirmed using additional human proteome databases[42,43] (Figure 4B). Using a secretome pool merged by the cell proteome and the Human Protein Atlas[44] databases, we refined the enriched FOXA1-CGS_Secretome (n = 165) within CGS_UP genes (Figure 4C).

Using our prior RNA-seq data of TamR cells upon FOXA1/ER small interfering RNA (siRNA) knockdown (KD),[20] we found that FOXA1-CGS_Secretome was significantly enriched in DN genes upon FOXA1 KD in MCF7-TamR but not P cells (Figures 4D and 4E). To better understand the role of ER in activating H-FOXA1 signaling, we identified Secretome14 as a 14-gene signature that was DN upon ER and FOXA1 KD preferentially in TamR vs. P cells (Figures 4F–4H). These findings were in line with the observation of marked enhancement of FOXA1 binding and lesser but significant enhancement of ER binding at the Secretome14 gene loci in TamR vs. P cells treated with Tam (Figures S6A and S6B). Enhanced FOXA1 binding was observed at individual Secretome14 gene loci in TamR vs. P cells treated with E2 or Tam, whereas half of the gene loci harbored increased ER binding in TamR and P cells treated with Tam vs. P cells treated with E2 (Figures S6C and S6D). Secretome14 gene expression and secreted protein levels (5 measured by ELISA) were largely increased in TamR vs. P cells treated with E2 or Tam (Figures S7A and S7B), suggesting that the increased ER binding at the gene loci in E2-treated P cells is possibly involved in gene repression.[45] In addition, we found that secretion of the four secretome factors (ANG, EDN1, GOLM1, and IL-8) was significantly UP in MCF7-P cells upon ectopic FOXA1 vs. YFP OE (Figure S7C), further supporting a role of H-FOXA1 in activating secretome gene expression. Importantly, GO analysis of Secretome14 reveals an association of cellular response to the tumor microenvironment (TME) and cancer pathways, including EGFR-dependent endothelin signaling and the AP-1 TF network (Figures S8A and S8B). By analyzing the RNA-seq data of the clinical ER+ metastatic cohort,[46] we found that gene expression of several known receptors of the Secretome14 factors (e.g., IL-8 and EDN1) was significantly elevated in ER+ metastases vs. ER+ primary tumors (Figure S8C). These findings suggest a potential role of Secretome14 in modulating the TME by interacting with their cognate receptors in adjacent epithelial and non-epithelial cell populations.

We have shown previously that AP-1 is a key mediator of EndoR[47] and that its motif is highly enriched at H-FOXA1-engaged enhancers in TamR cells.[29] Using two MCF7-TamR clones engineered with Dox-inducible dominant-negative c-Jun expression, we found that all but one Secretome14 gene were substantially DN upon dominant-negative c-Jun expression (Figure S9A). Furthermore, analyzing the c-Jun transcriptomic and cistromic data obtained from the P/TamR model,[48] we found that 12 of the Secretome14 genes were DN upon c-Jun shRNA KD in

(E and F) GSEA plots showing the enrichment of FOXA1-CGS_UP genes in the transcriptome of ZR75-1 and T47D cells with ectopic FOXA1 OE. NES, normalized enrichment score.

(G) Western blots for FOXA1, ER, and PR proteins in four ER+ BC cell models with their EndoR derivatives. Also included is FOXA1 densitometry after normalization using β-actin.

(H) Bar charts showing the enrichment score (ES) of the FOXA1-CGS, calculated by single-sample (ss) GSEA using the RNA-seq data with duplicates for each cell model. FOXA1/ER/PR expression (positive or negative) and FOXA1 UP status (EndoR vs. P) based on the western blots are shown in the top panel.

(I) Quantification of the z-centered ssGSEA ES of the FOXA1-CGS across three defined categories of cell models. The box was plotted by mean ± SEM, with whiskers extended to the highest and lowest values. The p value was determined using a pairwise t test with multiple test corrections.

See also Figures S4 and S5.

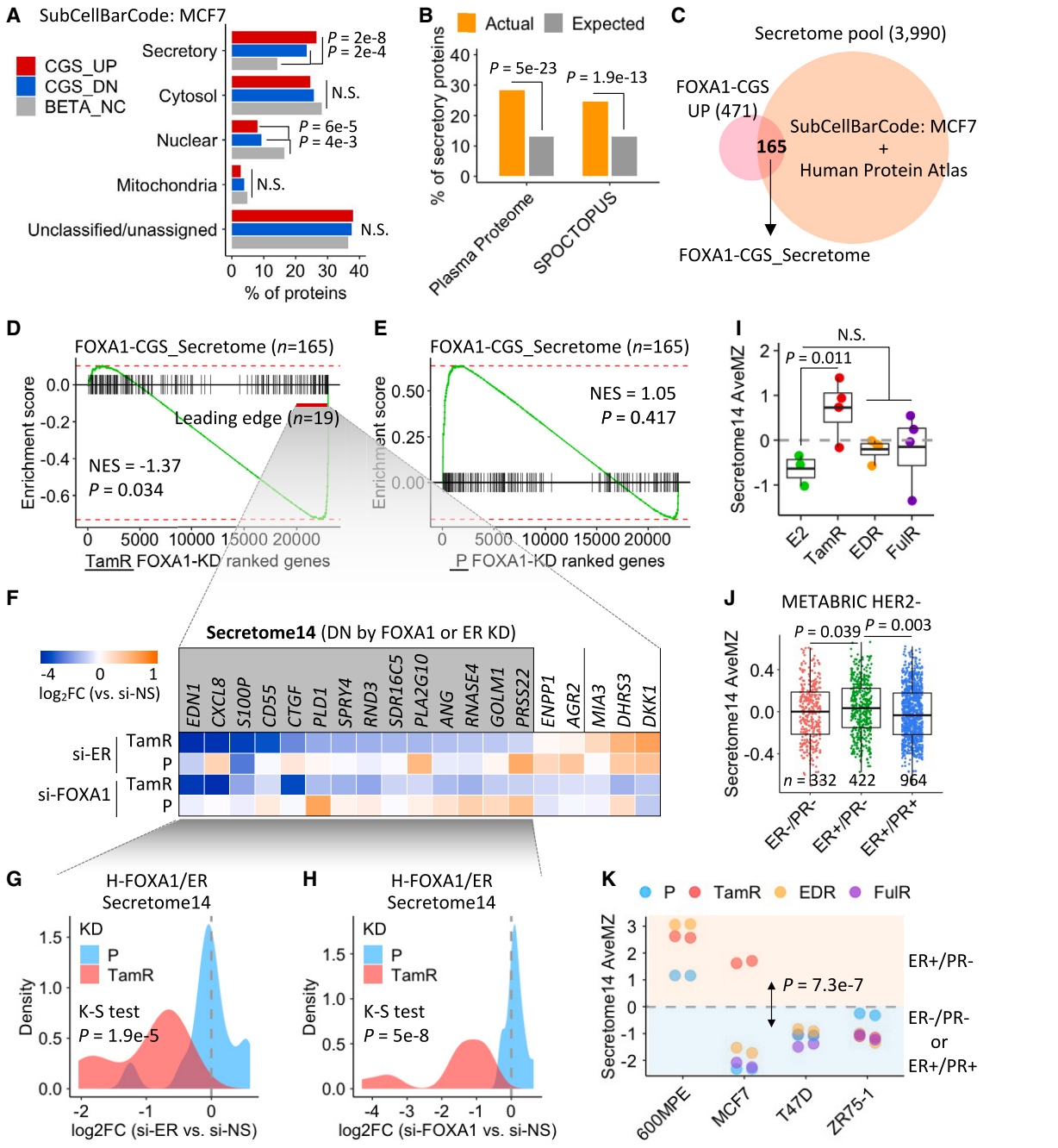

Figure 4. The FOXA1-CGS is enriched for an H-FOXA1/ER-dependent secretome in ER+ EndoR cells

(A) Bar charts showing subcellular distribution of the proteins encoded by the FOXA1-CGS genes using the MCF7 proteome SubCellBarCode data.[41] NC, no change.

(B) Bar charts showing the actual and expected proportions of the FOXA1-CGS_UP genes encoding secretory proteins defined by Plasma Proteome[42] and SPOCTOPUS.[43]

(C) Venn diagram depicting the FOXA1-CGS_Secretome annotated by the secretome pool merged by the MCF7 SubCellBarCode proteome and the secretome classified by the Human Protein Atlas v.19 (https://www.proteinatlas.org).

(D and E) GSEA plots showing enrichment of the FOXA1-CGS_Secretome genes in the transcriptome of MCF7-TamR and P cells upon FOXA1 knockdown (KD).

(F) Heatmaps showing expression log2 fold change (FC) of the leading-edge gene (from D) in TamR and P cells upon ER or FOXA1 KD vs. nonspecific (NS) KD. The subpanel of Secretome14 that is DN upon ER and FOXA1 KD in TamR cells is shaded in gray.

(G and H) Density plots displaying the preferential changes in Secretome14 gene expression in TamR vs. P cells upon ER or FOXA1 KD. The p value was determined using a two-sided Kolmogorov-Smirnov test.

(I) Quantification of Secretome14 expression, assessed by the average modified *Z* score (AveMZ), across MCF7 E2-treated and EndoR xenograft tumors.

(legend continued on next page)

TamR cells (Figure S9A, right panel). Accordingly, c-Jun binding was markedly increased at the FOXA1 binding sites nearby the Secretome14 gene loci in TamR vs. P cells (Figures S9B–S9D), suggesting a FOXA1/ER/AP-1-dependent mechanism in activating Secretome14 in EndoR cells. Next, we used the average modified *Z* score (AveMZ) to assess the Secretome14 signature in MCF7 EndoR xenograft tumors.[49] Compared with the E2-treated tumors, Secretome14 expression was significantly increased in TamR but not EDR and FulR xenograft tumors (Figure 4I). Of note, in contrast to ER+/PR− TamR tumors, FulR tumors are ER−/PR−, and EDR tumors are ER+/PR+ that maintain luminal gene signatures.[38,49] Analyzing gene expression data of HER2− tumors from the Molecular Taxonomy of Breast Cancer International Consortium (METABRIC), we found a significant increase in Secretome14 in ER+/PR− vs. ER−/PR− or ER+/PR+ tumors (Figure 4J), suggesting that Secretome14 correlates with ER/PR status in primary untreated tumors. Likewise, Secretome14 expression was also significantly higher in the ER+/PR− than the ER−/PR− and ER+/PR+ EndoR cell models (Figure 4K).

High Secretome14 expression predicts poor outcomes of ER+ BC treated with endocrine therapy

To further explore the clinical relevance of the H-FOXA1/ER-dependent Secretome14, we interrogated the METABRIC clinicopathologic data.[50,51] We found that high Secretome14 expression robustly predicted shorter BC-specific survival (BCSS) in ER+ BC receiving endocrine therapy without chemotherapy (Figure 5A) but not in ER+ BC with no endocrine therapy (Figure 5B). In the same setting of ER+ BC, multivariate analyses revealed that high Secretome14 expression independently decreased BCSS within a relatively longer follow-up time frame (Figure 5C), indicating a molecular signature linked to a late recurrence. In addition, high Secretome14 expression robustly predicted shorter DRFS in ER+ BC receiving endocrine therapy without chemotherapy (Figure 5D); a lesser significance was observed in ER+ BC with no endocrine therapy (Figure 5E). In contrast, no significance was observed for local RFS stratified by Secretome14 in ER+ BC with or without endocrine therapy (Figures S10A and S10B). Like tumor stage and LN positivity, high Secretome14 independently predicted decreased DRFS in 5- and 15-year follow-up (Figure 5F). These findings were reiterated by analyzing a second gene expression megaset, KM-plotter,[52] in which high Secretome14 expression was significantly associated with poor outcomes in ER+ BC receiving endocrine therapy without chemotherapy but not those without endocrine therapy (Figures S10C–S10F).

Using the multivariate regression model, we identified *S100P* and *CD55*, which independently predicted poor outcomes in ER+ BC receiving endocrine therapy without chemotherapy within 5 and 15 years (Figures 5G, 5H, S10G, and S10H). *S100P* and *CD55* predicted poor DRFS (Figures S10I and S10J), suggesting an essential role of these two factors in ER+ BC metastasis engendered by H-FOXA1/ER signaling.

Secretome14 correlates with FOXA1 expression and escalates in ER+ metastatic tumors

We then asked whether Secretome14 expression is altered during ER+ disease progression. We interrogated the recent clinical sequencing study, as mentioned above.[46] Compared with ER+ primary tumors, Secretome14 expression was markedly elevated in ER+ metastases (mets) (Figure 6A). Secretome14 expression was positively correlated with *FOXA1* mRNA levels in ER+ primary tumors and ER+ mets (Figures 6B and 6C). *FOXA1* genetic aberration (amplification or missense mutations), as reported previously,[21,23,53] was identified in 11% of ER+ mets, in which both Secretome14 and FOXA1 expression levels were higher than the mets harboring wild-type (WT) *FOXA1* (Figures 6D and S11A). Similar to a previous report,[54] *ESR1* mutations were identified in 26% of the ER+ mets; however, no difference in Secretome14 expression was observed in *ESR1*-mutant vs. WT mets irrespective of *FOXA1* status (Figure 6E). When comparing Secretome14 expression longitudinally for the same patient, Secretome14 expression was UP in *FOXA1*-WT mets vs. matched primary tumors irrespective of the *ESR1* status (Figure 6F). These findings suggest that, in a subset of *FOXA1*-WT ER+ mets, the increase in Secretome14 could be driven by other mechanisms, including *ESR1* mutations, which have been shown to be largely mutually exclusive to the *FOXA1* aberrations in ER+/HER2− metastatic BC.[23,29]

Among individual Secretome14 genes, we identified *S100P*, *GOLM1*, and *CXCL8* as the top three highly UP genes in ER+ mets vs. ER+ primary tumors, with a similar pattern of increase also seen in ER+ mets vs. a primary tumor from the same patient (Figures 6G and S11B). The fact that the Secretome14 genes were not equally increased in ER+ mets vs. primary tumors is possibly due to their varied expression patterns linked to different biological roles in disease progression. Nevertheless, FOXA1 expression level was positively correlated with most Secretome14 genes in ER+ mets and, to a lesser extent, in ER+ primary tumors (Figures 6H and 6I), suggesting a continuing role of H-FOXA1 in activating Secretome14 in ER+ mets.

Because we have shown previously that H-FOXA1 mediates EndoR partially by inducing IL-8 (encoded by the *CXCL8* gene),[20] we asked whether IL-8 secretion has a paracrine effect on endocrine-sensitive cells. We found that MCF7-P cells, secreting neglectable levels of IL-8, became more migrative when cultured with conditioned medium collected from P cells expressing ectopic IL-8 vs. YFP (Figures S11C and S11D). Importantly, in TamR cells expressing H-FOXA1 and IL-8 but not P cells, an IL-8 neutralizing antibody led to significant and dose-dependent suppression of cell migration (Figures S11E and S11F). Overall, these data indicate that high Secreteome14

(J) Quantification of Secretome14 AveMZ across METABRIC HER2− BC with defined ER/PR status.
(K) Dot plots showing Secretome14 AveMZ across four EndoR cell models (each in duplicates) with defined ER/PR status. The p value was determined using an unpaired two-sample t test.
For (A) and (B), the *p* value was determined using a chi-square test with Bonferroni multicomparison adjustment. N.S., non-significant. For (I) and (J), the box was plotted by mean ± SEM, and the *p* value was determined using a pairwise t test with multiple test corrections. See also Figures S6–S9.

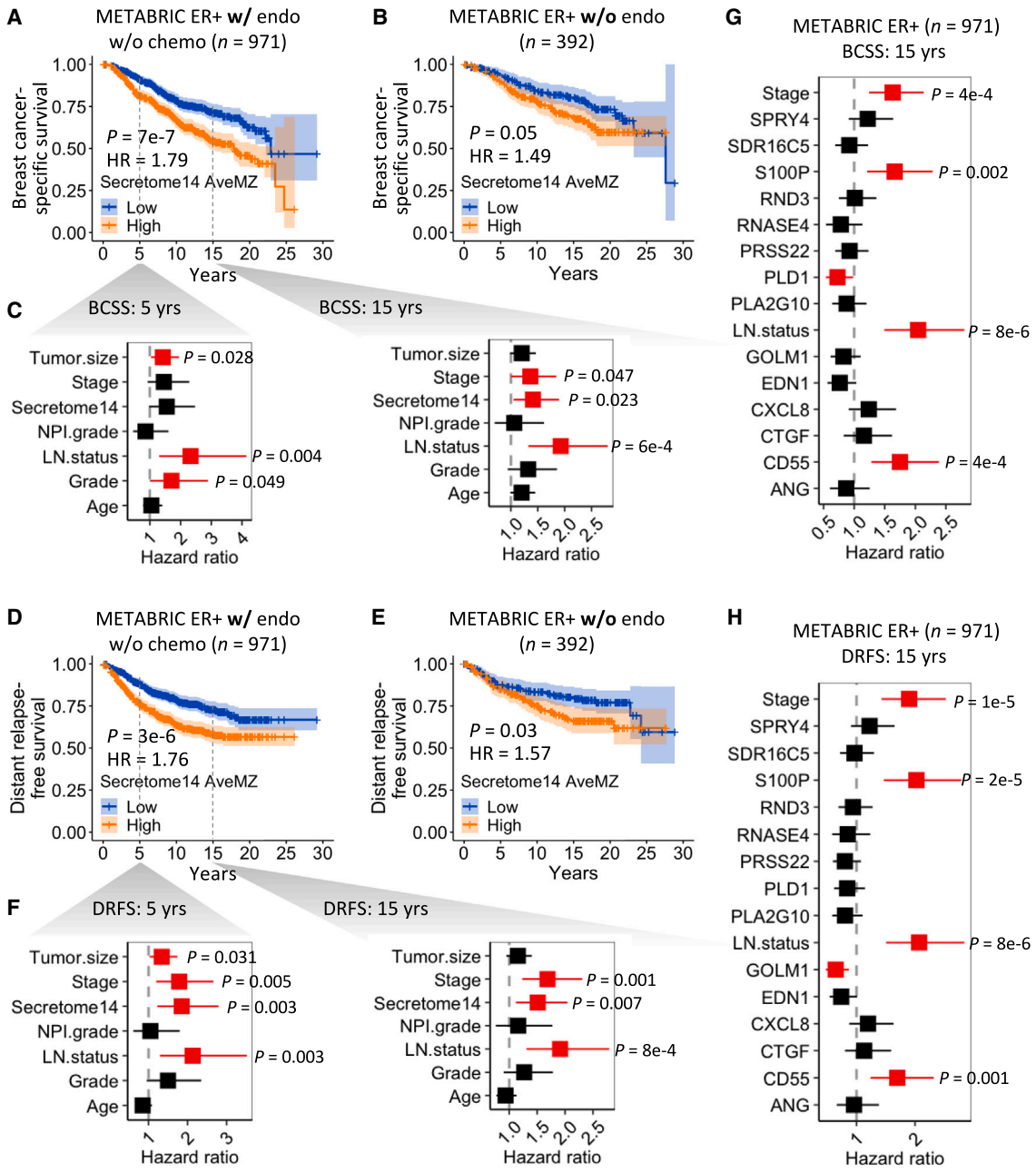

Figure 5. Secretome14 predicts poor outcomes of ER+ BC treated with endocrine therapy (ET)

(A and B) Kaplan-Meier plots depicting BC-specific survival (BCSS) of ER+ BC patients treated with ET and no chemotherapy and of patients without ET, stratified by median level of Secretome14 expression. The 95% confidence interval (CI) is depicted in colors for point estimates hereafter. The p value and hazard ratio (HR) were calculated hereafter using a likelihood ratio test and Wald estimates in the Cox proportional hazards model.

(C) Forest plots for HR of Cox multivariate analyses. Factors contributing to BCSS within 5- and 15-year follow-up are indicated by the red boxes, with $p < 0.05$. NPI, Nottingham prognostic index.

(D and E) Kaplan-Meier plots depicting DRFS of ER+ BC patients treated with ET and no chemotherapy and of patients without ET, stratified by median level of Secretome14 expression.

(F) Forest plots for HR of Cox multivariate analyses. Factors contributing to DRFS within 5- and 15-year follow-up are indicated by the red boxes, with $p < 0.05$.

(G and H) Forest plots for HR of Cox multivariate analyses. Single Secretome14 genes and clinicopathologic factors contributing to BCSS and DRFS within 15-year follow-up are indicated by the red boxes, with $p < 0.05$.

See also Figure S10.

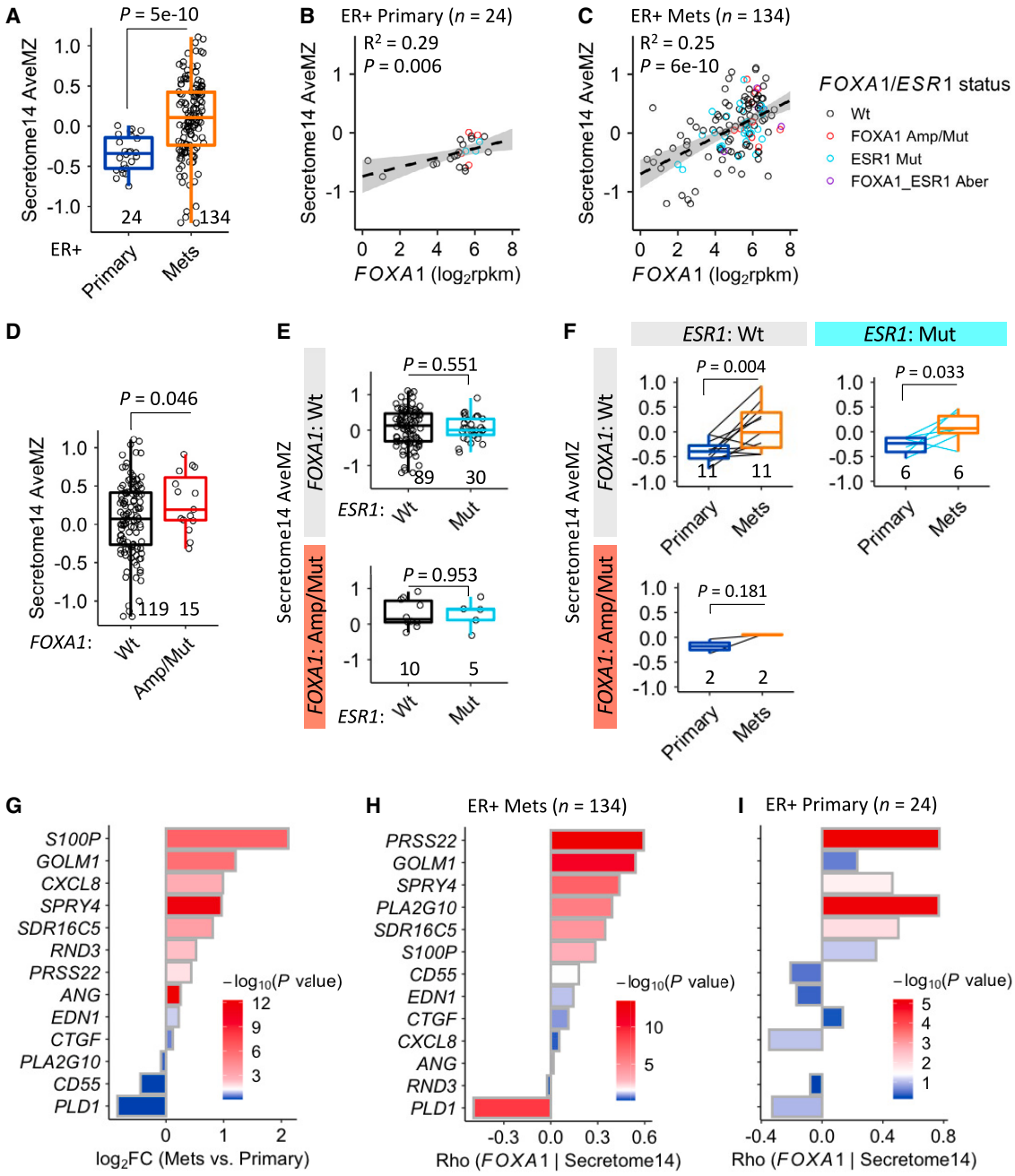

Figure 6. Secretome14 correlates with FOXA1 expression and escalates in ER+ mets

(A) Quantification of Secretome14 expression in ER+ mets vs. ER+ primary tumors. The p value was determined using Welch's t test for samples with unequal variance.

(B and C) Scatterplots depicting correlation between *FOXA1* mRNA and Secretome14 expression levels in ER+ primary tumors and ER+ mets. The p value was determined using a Pearson correlation coefficient test. The genetic status of *FOXA1* and *ESR1* is denoted in the right panel. WT, wild-type; Amp, amplification; Mut, mutant; Aber, aberration.

(D) Quantification of Secretome14 expression in ER+ mets harboring Amp/Mut vs. WT *FOXA1*.

(E) Quantification of Secretome14 expression in ER+ mets (stratified by the *FOXA1* status in the top and bottom) harboring Mut vs. WT *ESR1*.

(F) Changes in Secretome14 expression in ER+ mets (stratified by *FOXA1* and *ESR1* status) vs. their matched ER+ primary tumors. The number of matched pairs in each group is indicated. The p value was determined using a paired two-sample t test.

(G) Expression changes of single Secretome14 genes in ER+ mets vs. ER+ primary tumors. Scaled color (split in white corresponding to p = 0.05) denotes a transformed p value calculated by unpaired two-sample t test.

(legend continued on next page)

expression is associated with ER+ metastatic BC via a potential role in initiating and/or sustaining the metastatic phenotypes of EndoR cells.

Enhanced cistromic ER binding is coupled with ER transcriptional reprogramming of Secretome14

We next asked whether the H-FOXA1/ER-regulated Secretome14 is also regulated by the mutant ER, which has been shown to promote a pro-metastatic phenotype.[55,56] We analyzed the ChIP-seq and RNA-seq data derived from MCF7 cells with ectopic mutant ER OE.[55] Compared with E2-treated WT cells, ER binding was significantly increased in the enhancer regions near the transcription start site (TSS) of the Secretome14 genes in ER-Y537S mutant-expressing cells on either ED or E2 treatment; a smaller increase was observed in cells expressing the D538G mutant (Figure 7A). Interestingly, whereas Secretome14 expression was repressed upon E2 treatment, a marked increase was seen upon ER-Y537S mutant OE under ED and E2 treatment conditions, supporting E2-independent constitutive activation of mutant ER driving Secretome14 expression (Figure 7B). The weaker effect of the ER-D538G mutant on Secretome14 expression is possibly due to its lower binding affinity and allele-specific activity in comparison with the Y537S mutant, which is linked to more aggressive phenotypes and poorer outcomes in ER+ BC.[55,57]

Because high GFR and cytokine signaling also alters the ER cistrome associated with EndoR,[13,15,58] we assessed the changes in cistromic ER binding at Secretome14 in MCF7 cells treated with mitogens and in ER+/HER2− tumors with different prognoses[13] (Figure 7C). Upon mitogenic stimulation, ER and FOXA1 binding was significantly increased at the enhancer and promoter regions of the Secretome14 genes (Figures 7D and S12A–S12C). Whereas cistromic ER binding was absent in ER− tumors, the highest ER binding at Secretome14 was observed in ER+ mets, followed by ER+ primary tumors with poor vs. good prognosis (Figures 7E and S12D). Finally, we found that the cistromic ER binding profile of Secretome14 distinguished ER+ mets and ER+ primary tumors with poor prognosis (Figures 7F and S12E). Altogether, these data suggest that the H-FOXA1/ER-dependent Secretome14 is also driven by ER cistromic reprogramming, including via ligand-independent mutant ER and/or high GFR signaling in ER+ EndoR and metastatic BC.

DISCUSSION

Resistance to endocrine therapy is often associated with reactivation of ER signaling. As a key determinant of ER-chromatin binding and function, FOXA1 has been shown to be upregulated in EndoR cell models and ER+ metastatic BC,[13,20] but its interplay with ER to regulate genes in ER+ disease progression is not completely understood. Building on our earlier studies demonstrating that H-FOXA1 induces enhancer and transcriptional reprogramming in EndoR BC,[29] in this study we delineated the distinct role of H-FOXA1 in reprogramming the ER cistrome and transcriptome to promote EndoR ER+ metastatic BC. We identified the Secretome14 gene set as a key transcriptional target of the reprogrammed H-FOXA1/ER axis, capable of predicting a poor prognosis of ER+ BC patients treated with endocrine therapy. Moreover, we show that Secretome14 further escalates in ER+ metastatic BC, possibly via a regulation enacted convergingly by H-FOXA1, *ESR1* mutations, and high GFR/cytokine signaling (Figure 7G).

We have shown previously that H-FOXA1 induces EndoR and pro-metastatic phenotypes in ER+ BC cells.[20] In this study, using xenograft mouse models, we found that H-FOXA1 facilitated the occurrence of ER+ mets in Tam-treated tumors with no obvious influence on primary tumor endocrine response. Notably, the endogenous upregulation of FOXA1 in TamR tumors may mask the impact of exogenous H-FOXA1 on endocrine response in primary tumors. Future clinical studies using large cohorts will be needed to clarify whether the impact of H-FOXA1 on ER+ BC prognosis is associated with the type of endocrine therapy.

We found that H-FOXA1 markedly reduced genome-wide ER binding at regions enriched for estrogen-responsive *cis* elements. We have shown previously that H-FOXA1 reduces the expression of GATA3,[20] a luminal-specific TF that forms a positive cross-regulatory loop with ER in dictating the classic E2-dependent transcriptional network.[59,60] Therefore, this reduction of E2-responsive ER binding, linked to loss of GATA3, may skew luminal BC cells with a consequent ligand-independent or SERM-modulated transcriptome, which is further promoted via H-FOXA1-induced multiple oncogenic GFR signaling.[20] In androgen-responsive prostate cancer cells, ectopic FOXA1 OE increased androgen receptor (AR) genomic gain binding associated with a castration-resistant phenotype.[35] However, in endocrine-sensitive BC cells, we found that H-FOXA1 induced a small portion of ER gain binding, which was not further enhanced in TamR cells. Whether this is due to a discrepancy in FOXA1 interplay with ER vs. AR in hormone-related cancers, as suggested previously,[61] remains to be seen. Moreover, the cellular response to transient H-FOXA1 in P cells vs. FOXA1 accumulation in acquired TamR cells may also account for the discrepancy in hormone-related chromatin binding and interactions of ER and FOXA1, as suggested previously.[26–28]

Our integrative data analyses identified the H-FOXA1-induced CGS highly represented in other H-FOXA1 cell models of prostate and pancreatic cancers. All of these models shared a transcriptomic commonality associated with tumor aggressiveness and metastasis, suggesting a general role of H-FOXA1 in regulating pro-metastatic gene expression in cancers sharing an original endoderm lineage identity.[34] In ER+ BC, we identified the ER-dependent Secretome14 as a subset of the CGS enriched for genes encoding secretory proteins. Proteins secreted from cancer cells, collectively termed the cancer secretome, play a crucial role in tumor progression and therapy resistance.[62,63] We found that Secretome14 is

(H and I) Correlation between expression levels of *FOXA1* and single Secretome14 genes in ER+ mets and ER+ primary tumors. Scaled color (split in white corresponding to p = 0.05) denotes a transformed p value calculated by a Spearman correlation coefficient test.
For (D) and (E), the p value was determined using a Wilcoxon rank-sum test. See also Figure S11.

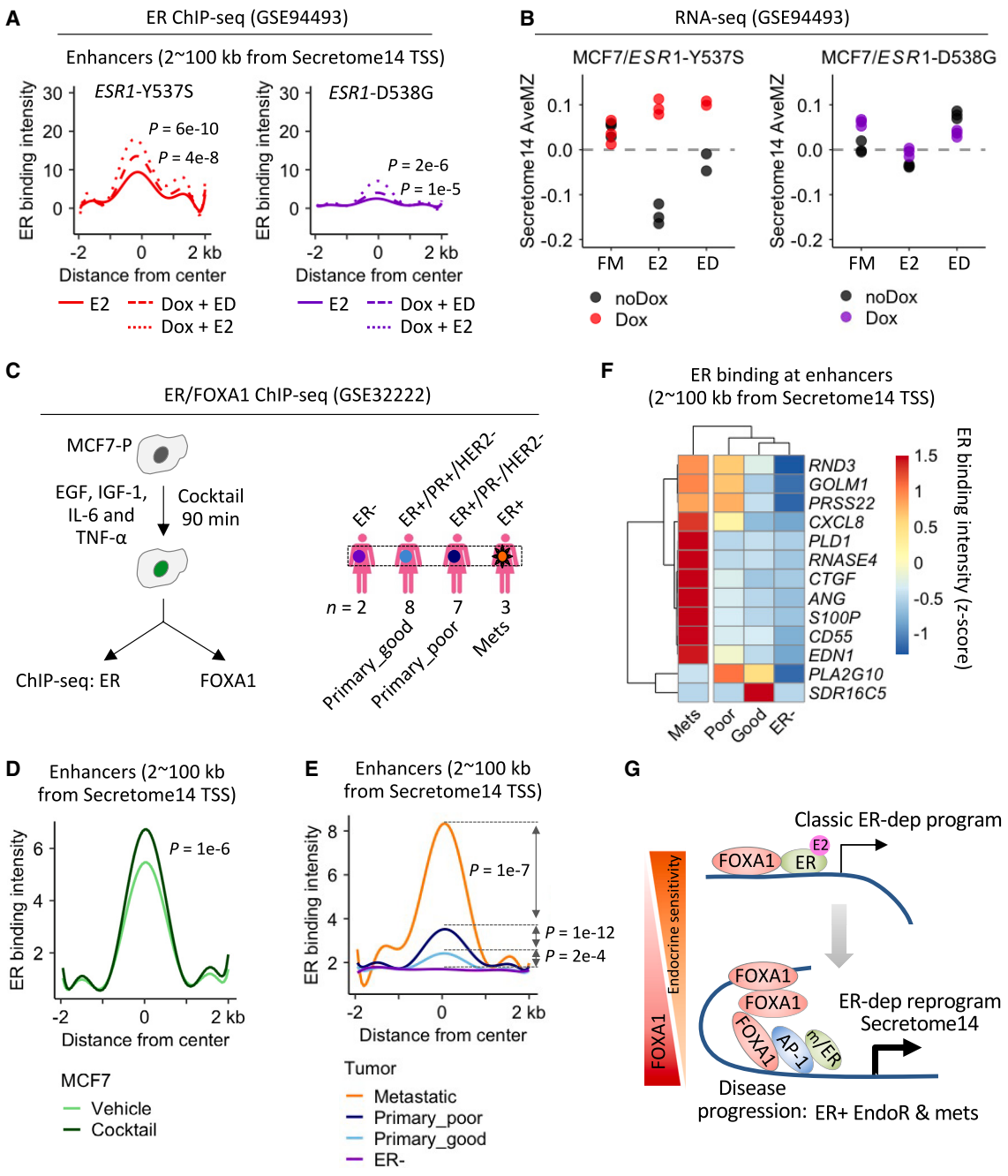

Figure 7. Enhanced ER binding and reprogramming occurs at the Secretome14 gene loci in ER+ cell models and clinical tumors

(A) Average ER binding intensity at the Secretome14 gene enhancers in MCF7 cells upon E2 or E2 vs. ED in the presence of Dox inducing ectopic Mut ER (Y537S or D538G) OE.

(B) Dot plots showing Secretome14 expression in MCF7 cells ±Dox to induce ectopic Mut ER (Y537S or D538G) OE in full medium (FM) or upon E2 or ED treatment.

(C) Schematic of the ChIP-seq experiments using MCF7 cells and clinical BC samples (as in Ross-Innes et al.[13]).

(D and E) Average ER binding intensity at the Secretome14 gene enhancers in MCF7 cells treated with cocktail and in the BC cohort.

(F) Heatmap of hierarchical clustering of the aggregated ER binding intensity at the single Secretome14 gene enhancers across ER+ mets, ER+ tumors with poor or good prognosis, and ER− tumors.

(G) Model depicting ER-dependent (dep) reprogramming activated by the H-FOXA1/ER transcriptional axis to promote BC EndoR and metastasis.

For (A), (D), and (E), the p value was determined using a paired two-sample t test. See also Figure S12.

highly dependent on ER in TamR vs. P cells and activated in ER+/PR− EndoR cell models. Notably, AP-1 is also engaged in H-FOXA1/ER-dependent Secretome14 activation by accumulating at FOXA1-bound genomic regions in TamR vs. P cells, confirming the importance of AP-1 in ER-dependent transcriptional reprogramming.[15,20] Our findings suggest a role of H-FOXA1 in activating genes encoding secretome factors in EndoR and metastatic BC, reminiscent of previously described FOXA1 functions in metabolic and secretory activities of pancreas β cells and intestinal epithelium.[64,65] S100P and CTGF, two Secretome14 factors, have been shown to activate integrin and downstream AKT/ERK signaling to promote lung and BC cell migration and invasion.[66,67] Because the cancer secretome is involved in many hallmarks of cancers,[68] Secretome14 could convey H-FOXA1-induced GFR and integrin signaling[20] to support tumor metastasis, as observed in our xenograft mouse model. Additional studies will be required to delineate mechanistically how different Secretome14 members collectively amplify H-FOXA1/ER signaling to promote EndoR ER+ metastatic BC.

The clinical relevance of our findings was validated by the fact that Secretome14 predicts a poor prognosis of ER+ BC patients treated with endocrine therapy. Elevated serum and tumor-associated IL-8 has been shown to correlate with enhanced intratumor neutrophils and reduced clinical benefit of immune checkpoint inhibitors in patients with advanced cancers.[69,70] Using multivariate regression modeling, we identified *S100P* and *CD55* as two independent risk factors contributing to a poor outcome for ER+ BC patients. S100P belongs to the calcium-binding S100 family, and its plasma level is useful in predicting a poor prognosis of metastatic BC.[71] CD55 is a membrane-bound glycoprotein protecting cells from complement-mediated lysis.[72] CD55 OE is an independent risk factor for recurrence in BC patients receiving adjuvant trastuzumab,[73] and targeting CD55 has been shown to potentiate antibody-based anti-HER2 therapies.[74] We noticed that, whereas CD55 basal levels in ER+ primary tumors predict a poor patient outcome, it is one of the few secretome genes downregulated in ER+ mets vs. primary tumors, suggesting an inconsistent expression pattern of individual Secretome14 genes with discrete functionalities in ER+ disease progression, a finding that needs further investigation. Our findings indicate clinical relevance and potential values of Secretome14, individually or collectively as a molecular signature, when treating ER+ EndoR metastatic BC or circumventing the development of micrometastasis in the adjuvant setting.

Moreover, we demonstrated that Secretome14 was further increased in ER+ mets vs. ER+ primary tumors. Compared with their corresponding primary tumors, Secretome14 was elevated in the ER+ mets harboring WT-*FOXA1* irrespective of the *ESR1* mutations. ChIP-seq analyses of the *ESR1*-mutant cell models suggest that Secretome14 is also activated by the mutant ER, particularly the Y537S allele, which has been reported to be associated with more aggressive phenotypes and a poor prognosis of ER+ BC.[55,57] Because the *ESR1* mutations have been found to be largely mutually exclusive to the *FOXA1* aberrations in ER+/HER2− metastatic BC,[23,29] these findings might suggest a shared mechanism whereby genetic/epigenetic aberrations of *FOXA1* or *ESR1* activate Secretome14 as a part of ER reprogramming in EndoR BC progression. Notably, genetic aberrations may also adopt epigenetic mechanisms to modulate the ER-dependent transcriptome. Recent studies have revealed that *ARID1A*-inactivating mutations, enriched in ER+/HER2− metastatic BC, modulate the SWI/SNF chromatin remodeling complex to promote an ER-dependent but less luminal-specific transcriptional program.[30,31] It will be interesting in future studies to investigate whether ER reprogramming induced by H-FOXA1, including via activating *FOXA1* mutations, can be epigenetically modulated via interplay with the SWI/SNF complex.

In summary, our results demonstrate the important role of H-FOXA1 in promoting ER+ BC metastasis and provide, at least partly, a molecular basis by which H-FOXA1-induced ER reprogramming activates a pro-metastatic secretome. Because of the evolving role of ER in mediating high FOXA1 signaling, our findings suggest that blocking H-FOXA1/ER reprogramming with more potent ER degraders and potential epigenetic interventions may be an attractive approach to prevent and treat EndoR ER+ metastatic BC.

Limitations of the study

Although we were able to link Secretome14 expression to reprogrammed H-FOXA1/ER signaling and their clinical importance, our study did not fully address the role of Secretome14 in promoting H-FOXA1-induced EndoR tumor metastasis as shown in our mouse model. The underlying mechanisms of Secretome14, as a whole or individuals, influencing adjacent epithelial and other cell types, including the immune cell populations in ER+ tumor metastasis, are still unclear. Further functional and genomic studies in preclinical models and clinical specimens will help to determine how Secretome14 mediates H-FOXA1 signaling, including by engaging the TME in advanced ER+ BC.

STAR★METHODS

Detailed methods are provided in the online version of this paper and include the following:

- KEY RESOURCES TABLE
- RESOURCE AVAILABILITY
  - Lead contact
  - Materials availability
  - Data and code availability
- EXPERIMENTAL MODELS AND SUBJECT DETAILS
  - Cell culture
  - Xenograft mouse model
- METHOD DETAILS
  - *In vivo* tumor growth and metastasis modeling
  - ChIP-seq
  - RNA-seq
  - Immunohistochemistry
  - Western blotting
  - Preparation of conditioned medium
  - ELISA
  - Migration assay

- ChIP-seq data analysis
- RNA-seq and microarray data analysis
- Motif enrichment analysis
- Genomic motif scanning and positional gene expression analysis
- Binding and Expression Target Analysis (BETA)
- Ontology annotation, gene set enrichment analysis (GSEA), and single-sample (ss) GSEA
- Unsupervised hierarchical clustering
- Secretome enrichment analysis
- Calculation of average modified *Z* score (AveMZ)
- METABRIC and KM-plotter data analyses
- Target gene set *cis*-regulatory TF binding analysis

● QUANTIFICATION AND STATISTICAL ANALYSIS

- Statistical analyses

SUPPLEMENTAL INFORMATION

Supplemental information can be found online at https://doi.org/10.1016/j.celrep.2023.112821.

ACKNOWLEDGMENTS

This work was supported by CPRIT grant RP190398 (to R.S. and X.F.), DOD Breakthrough Award W81XWH-14-1-0326 (to X.F.), and the Breast Cancer Research Foundation (BCRF 17-143, BCRF 18-145, 19-145, 20-145, and 21-145 to R.S. and C.K.O.). Research reported in this study was also supported by NCI grant P30-CA125123 and CA008748 (to C.K.O.), NIH SPORE grant P50CA186784 (to C.K.O. and R.S.), Susan G. Komen Grant CCR15333343 (to N.W.), The V Foundation (to N.W.), The Breast Cancer Alliance (to N.W.), The Cancer Couch Foundation (to N.W.), and the 2020-4.1.1.-TKP2020 grant of the Ministry for Innovation and Technology Hungary (to B.G.). This project was supported in part by the Genomic and RNA Profiling Core at Baylor College of Medicine (BCM) with funding from NCI (P30CA125123) and CPRIT (RP200504) grants and by the Cytometry and Cell Sorting Core at BCM with funding from a CPRIT Core Facility Support Award (RP180672) and the NIH (CA125123 and RR024574) and assistance from Joel M. Sederstrom. We thank Dr. George Miles for assistance with reviewing IHC slides and Dr. Gary Chamness for reviewing this manuscript. We thank Michael Dehart for assistance with computational HPC at the BCM Cancer Center.

AUTHOR CONTRIBUTIONS

X.F. and R.S. conceived and supervised the project. X.F., R.S., R.P., C-.C.L., C.D.A., S.N., L.Q., M.J.S., T.M., M.L.C., V.S., and M.G. contributed to the experimental design and/or experiments. X.F., C.D.A., C.G., and R.S. contributed to data analyses. B.G. provided the KM-plotter dataset. O.C. and N.W. provided the clinical RNA-seq and target genomic profiles and assisted with data analysis. A.N. and R.J. conducted the cell line RNA-seq and analysis. X.F., M.J.S., J.V., M.V.T., M.F.R., C.K.O., and R.S. wrote the manuscript with input from other authors.

DECLARATION OF INTERESTS

C.K.O. is a consultant/advisory board member for AstraZeneca, GlaxoSmithKline, Pfizer, Puma Biotechnologies, and Tolmar and on the Data Monitoring Committee for Eli Lilly. R.S. has received research support (to institute) from Puma Biotechnology, Gilead Sciences, and AstraZeneca; is a consultant/advisor of MacroGenics; holds patents, royalties, and other intellectual property from Wolters Kluwer/UpToDate; and has a patent pending (via institution; NRF Ref. BAYM.P0312US.P1-1001123973 "A multiparameter classifier to predict response to HER2-targeted therapy without chemotherapy in HER2-positive breast cancer") with no revenue received. N.W. is a consultant/advisor for Eli Lilly and AstraZeneca, a member of the scientific advisory board and stockholder for Relay Therapeutics, and a member of the scientific advisory board and stockholder for Flare Therapeutics. He has previously received research support from Novartis and Puma Biotechnology, consulted with Novartis, and consulted with Foundation Medicine. R.J. has received research funding from Pfizer. M.F.R. has received research support from Pfizer and consults with Genentech, Novartis, Daiichi, AstraZeneca, Seagen, and MacroGenics. M.G. is a consultant/advisor for Eli Lilly, MSD, Novartis, Pfizer, Roche, and Seagen.

Received: November 17, 2021
Revised: November 3, 2022
Accepted: July 3, 2023
Published: July 18, 2023

REFERENCES

1. Huang, B., Warner, M., and Gustafsson, J.Å. (2015). Estrogen receptors in breast carcinogenesis and endocrine therapy. Mol. Cell. Endocrinol. *418*, 240–244. https://doi.org/10.1016/j.mce.2014.11.015.
2. Brisken, C., and O'Malley, B. (2010). Hormone action in the mammary gland. Cold Spring Harbor Perspect. Biol. *2*, a003178. https://doi.org/10.1101/cshperspect.a003178.
3. Reinert, T., de Paula, B., Shafaee, M.N., Souza, P.H., Ellis, M.J., and Bines, J. (2018). Endocrine therapy for ER-positive/HER2-negative metastatic breast cancer. Chin. Clin. Oncol. *7*, 25. https://doi.org/10.21037/cco.2018.06.06.
4. Osborne, C.K., and Schiff, R. (2011). Mechanisms of endocrine resistance in breast cancer. Annu. Rev. Med. *62*, 233–247. https://doi.org/10.1146/annurev-med-070909-182917.
5. Nardone, A., De Angelis, C., Trivedi, M.V., Osborne, C.K., and Schiff, R. (2015). The changing role of ER in endocrine resistance. Breast *24*, S60–S66. https://doi.org/10.1016/j.breast.2015.07.015.
6. O'Hara, J., Vareslija, D., McBryan, J., Bane, F., Tibbitts, P., Byrne, C., Conroy, R.M., Hao, Y., Gaora, P.Ó., Hill, A.D.K., et al. (2012). AIB1:ERalpha transcriptional activity is selectively enhanced in aromatase inhibitor-resistant breast cancer cells. Clin. Cancer Res. *18*, 3305–3315. https://doi.org/10.1158/1078-0432.CCR-11-3300.
7. Torres-Arzayus, M.I., Zhao, J., Bronson, R., and Brown, M. (2010). Estrogen-dependent and estrogen-independent mechanisms contribute to AIB1-mediated tumor formation. Cancer Res. *70*, 4102–4111. https://doi.org/10.1158/0008-5472.CAN-09-4080.
8. Schiff, R., Massarweh, S., Shou, J., and Osborne, C.K. (2003). Breast cancer endocrine resistance: how growth factor signaling and estrogen receptor coregulators modulate response. Clin. Cancer Res. *9*, 447S–454S.
9. Massarweh, S., Osborne, C.K., Creighton, C.J., Qin, L., Tsimelzon, A., Huang, S., Weiss, H., Rimawi, M., and Schiff, R. (2008). Tamoxifen resistance in breast tumors is driven by growth factor receptor signaling with repression of classic estrogen receptor genomic function. Cancer Res. *68*, 826–833. https://doi.org/10.1158/0008-5472.CAN-07-2707.
10. Formisano, L., Stauffer, K.M., Young, C.D., Bhola, N.E., Guerrero-Zotano, A.L., Jansen, V.M., Estrada, M.M., Hutchinson, K.E., Giltnane, J.M., Schwarz, L.J., et al. (2017). Association of FGFR1 with ERalpha maintains ligand-independent ER transcription and mediates resistance to estrogen deprivation in ER(+) breast cancer. Clin. Cancer Res. *23*, 6138–6150. https://doi.org/10.1158/1078-0432.CCR-17-1232.
11. Jeselsohn, R., De Angelis, C., Brown, M., and Schiff, R. (2017). The evolving role of the estrogen receptor mutations in endocrine therapy-resistant breast cancer. Curr. Oncol. Rep. *19*, 35. https://doi.org/10.1007/s11912-017-0591-8.
12. Jeselsohn, R., Cornwell, M., Pun, M., Buchwalter, G., Nguyen, M., Bango, C., Huang, Y., Kuang, Y., Paweletz, C., Fu, X., et al. (2017). Embryonic transcription factor SOX9 drives breast cancer endocrine

resistance. Proc. Natl. Acad. Sci. USA *114*, E4482–E4491. https://doi.org/10.1073/pnas.1620993114.

13. Ross-Innes, C.S., Stark, R., Teschendorff, A.E., Holmes, K.A., Ali, H.R., Dunning, M.J., Brown, G.D., Gojis, O., Ellis, I.O., Green, A.R., et al. (2012). Differential oestrogen receptor binding is associated with clinical outcome in breast cancer. Nature *481*, 389–393. https://doi.org/10.1038/nature10730.
14. Chi, D., Singhal, H., Li, L., Xiao, T., Liu, W., Pun, M., Jeselsohn, R., He, H., Lim, E., Vadhi, R., et al. (2019). Estrogen receptor signaling is reprogrammed during breast tumorigenesis. Proc. Natl. Acad. Sci. USA *116*, 11437–11443. https://doi.org/10.1073/pnas.1819155116.
15. Lupien, M., Meyer, C.A., Bailey, S.T., Eeckhoute, J., Cook, J., Westerling, T., Zhang, X., Carroll, J.S., Rhodes, D.R., Liu, X.S., and Brown, M. (2010). Growth factor stimulation induces a distinct ER(alpha) cistrome underlying breast cancer endocrine resistance. Genes Dev. *24*, 2219–2227. https://doi.org/10.1101/gad.1944810.
16. Hurtado, A., Holmes, K.A., Ross-Innes, C.S., Schmidt, D., and Carroll, J.S. (2011). FOXA1 is a key determinant of estrogen receptor function and endocrine response. Nat. Genet. *43*, 27–33. https://doi.org/10.1038/ng.730.
17. Carroll, J.S., Liu, X.S., Brodsky, A.S., Li, W., Meyer, C.A., Szary, A.J., Eeckhoute, J., Shao, W., Hestermann, E.V., Geistlinger, T.R., et al. (2005). Chromosome-wide mapping of estrogen receptor binding reveals long-range regulation requiring the forkhead protein FoxA1. Cell *122*, 33–43. https://doi.org/10.1016/j.cell.2005.05.008.
18. Lupien, M., Eeckhoute, J., Meyer, C.A., Wang, Q., Zhang, Y., Li, W., Carroll, J.S., Liu, X.S., and Brown, M. (2008). FoxA1 translates epigenetic signatures into enhancer-driven lineage-specific transcription. Cell *132*, 958–970. https://doi.org/10.1016/j.cell.2008.01.018.
19. Iwafuchi-Doi, M., Donahue, G., Kakumanu, A., Watts, J.A., Mahony, S., Pugh, B.F., Lee, D., Kaestner, K.H., and Zaret, K.S. (2016). The pioneer transcription factor FoxA maintains an accessible nucleosome configuration at enhancers for tissue-specific gene activation. Mol. Cell *62*, 79–91. https://doi.org/10.1016/j.molcel.2016.03.001.
20. Fu, X., Jeselsohn, R., Pereira, R., Hollingsworth, E.F., Creighton, C.J., Li, F., Shea, M., Nardone, A., De Angelis, C., Heiser, L.M., et al. (2016). FOXA1 overexpression mediates endocrine resistance by altering the ER transcriptome and IL-8 expression in ER-positive breast cancer. Proc. Natl. Acad. Sci. USA *113*, E6600–E6609. https://doi.org/10.1073/pnas.1612835113.
21. Razavi, P., Chang, M.T., Xu, G., Bandlamudi, C., Ross, D.S., Vasan, N., Cai, Y., Bielski, C.M., Donoghue, M.T.A., Jonsson, P., et al. (2018). The genomic landscape of endocrine-resistant advanced breast cancers. Cancer Cell *34*, 427–438.e6. https://doi.org/10.1016/j.ccell.2018.08.008.
22. Rheinbay, E., Parasuraman, P., Grimsby, J., Tiao, G., Engreitz, J.M., Kim, J., Lawrence, M.S., Taylor-Weiner, A., Rodriguez-Cuevas, S., Rosenberg, M., et al. (2017). Recurrent and functional regulatory mutations in breast cancer. Nature *547*, 55–60. https://doi.org/10.1038/nature22992.
23. Arruabarrena-Aristorena, A., Maag, J.L.V., Kittane, S., Cai, Y., Karthaus, W.R., Ladewig, E., Park, J., Kannan, S., Ferrando, L., Cocco, E., et al. (2020). FOXA1 mutations reveal distinct chromatin profiles and influence therapeutic response in breast cancer. Cancer Cell *38*, 534–550.e9. https://doi.org/10.1016/j.ccell.2020.08.003.
24. Parolia, A., Cieslik, M., Chu, S.C., Xiao, L., Ouchi, T., Zhang, Y., Wang, X., Vats, P., Cao, X., Pitchiaya, S., et al. (2019). Distinct structural classes of activating FOXA1 alterations in advanced prostate cancer. Nature *571*, 413–418. https://doi.org/10.1038/s41586-019-1347-4.
25. Adams, E.J., Karthaus, W.R., Hoover, E., Liu, D., Gruet, A., Zhang, Z., Cho, H., DiLoreto, R., Chhangawala, S., Liu, Y., et al. (2019). FOXA1 mutations alter pioneering activity, differentiation and prostate cancer phenotypes. Nature *571*, 408–412. https://doi.org/10.1038/s41586-019-1318-9.
26. Glont, S.E., Chernukhin, I., and Carroll, J.S. (2019). Comprehensive genomic analysis reveals that the pioneering function of FOXA1 is independent of hormonal signaling. Cell Rep. *26*, 2558–2565.e3. https://doi.org/10.1016/j.celrep.2019.02.036.
27. Swinstead, E.E., Miranda, T.B., Paakinaho, V., Baek, S., Goldstein, I., Hawkins, M., Karpova, T.S., Ball, D., Mazza, D., Lavis, L.D., et al. (2016). Steroid receptors reprogram FoxA1 occupancy through dynamic chromatin transitions. Cell *165*, 593–605. https://doi.org/10.1016/j.cell.2016.02.067.
28. Paakinaho, V., Swinstead, E.E., Presman, D.M., Grøntved, L., and Hager, G.L. (2019). Meta-analysis of chromatin programming by steroid receptors. Cell Rep. *28*, 3523–3534.e2. https://doi.org/10.1016/j.celrep.2019.08.039.
29. Fu, X., Pereira, R., De Angelis, C., Veeraraghavan, J., Nanda, S., Qin, L., Cataldo, M.L., Sethunath, V., Mehravaran, S., Gutierrez, C., et al. (2019). FOXA1 upregulation promotes enhancer and transcriptional reprogramming in endocrine-resistant breast cancer. Proc. Natl. Acad. Sci. USA *116*, 26823–26834. https://doi.org/10.1073/pnas.1911584116.
30. Xu, G., Chhangawala, S., Cocco, E., Razavi, P., Cai, Y., Otto, J.E., Ferrando, L., Selenica, P., Ladewig, E., Chan, C., et al. (2020). ARID1A determines luminal identity and therapeutic response in estrogen-receptor-positive breast cancer. Nat. Genet. *52*, 198–207. https://doi.org/10.1038/s41588-019-0554-0.
31. Nagarajan, S., Rao, S.V., Sutton, J., Cheeseman, D., Dunn, S., Papachristou, E.K., Prada, J.E.G., Couturier, D.L., Kumar, S., Kishore, K., et al. (2020). ARID1A influences HDAC1/BRD4 activity, intrinsic proliferative capacity and breast cancer treatment response. Nat. Genet. *52*, 187–197. https://doi.org/10.1038/s41588-019-0541-5.
32. Donaghey, J., Thakurela, S., Charlton, J., Chen, J.S., Smith, Z.D., Gu, H., Pop, R., Clement, K., Stamenova, E.K., Karnik, R., et al. (2018). Genetic determinants and epigenetic effects of pioneer-factor occupancy. Nat. Genet. *50*, 250–258. https://doi.org/10.1038/s41588-017-0034-3.
33. Wang, S., Sun, H., Ma, J., Zang, C., Wang, C., Wang, J., Tang, Q., Meyer, C.A., Zhang, Y., and Liu, X.S. (2013). Target analysis by integration of transcriptome and ChIP-seq data with BETA. Nat. Protoc. *8*, 2502–2515. https://doi.org/10.1038/nprot.2013.150.
34. Roe, J.S., Hwang, C.I., Somerville, T.D.D., Milazzo, J.P., Lee, E.J., Da Silva, B., Maiorino, L., Tiriac, H., Young, C.M., Miyabayashi, K., et al. (2017). Enhancer reprogramming promotes pancreatic cancer metastasis. Cell *170*, 875–888.e20. https://doi.org/10.1016/j.cell.2017.07.007.
35. Robinson, J.L.L., Hickey, T.E., Warren, A.Y., Vowler, S.L., Carroll, T., Lamb, A.D., Papoutsoglou, N., Neal, D.E., Tilley, W.D., and Carroll, J.S. (2014). Elevated levels of FOXA1 facilitate androgen receptor chromatin binding resulting in a CRPC-like phenotype. Oncogene *33*, 5666–5674. https://doi.org/10.1038/onc.2013.508.
36. Huang, D.W., Sherman, B.T., and Lempicki, R.A. (2009). Systematic and integrative analysis of large gene lists using DAVID bioinformatics resources. Nat. Protoc. *4*, 44–57. https://doi.org/10.1038/nprot.2008.211.
37. Liberzon, A., Birger, C., Thorvaldsdóttir, H., Ghandi, M., Mesirov, J.P., and Tamayo, P. (2015). The Molecular Signatures Database (MSigDB) hallmark gene set collection. Cell Syst. *1*, 417–425. https://doi.org/10.1016/j.cels.2015.12.004.
38. Nardone, A., Weir, H., Delpuech, O., Brown, H., De Angelis, C., Cataldo, M.L., Fu, X., Shea, M.J., Mitchell, T., Veeraraghavan, J., et al. (2019). The oral selective oestrogen receptor degrader (SERD) AZD9496 is comparable to fulvestrant in antagonising ER and circumventing endocrine resistance. Br. J. Cancer *120*, 331–339. https://doi.org/10.1038/s41416-018-0354-9.
39. Sanchez, C.G., Ma, C.X., Crowder, R.J., Guintoli, T., Phommaly, C., Gao, F., Lin, L., and Ellis, M.J. (2011). Preclinical modeling of combined phosphatidylinositol-3-kinase inhibition with endocrine therapy for estrogen receptor-positive breast cancer. Breast Cancer Res. *13*, R21. https://doi.org/10.1186/bcr2833.
40. Barbie, D.A., Tamayo, P., Boehm, J.S., Kim, S.Y., Moody, S.E., Dunn, I.F., Schinzel, A.C., Sandy, P., Meylan, E., Scholl, C., et al. (2009). Systematic RNA interference reveals that oncogenic KRAS-driven

cancers require TBK1. Nature *462*, 108–112. https://doi.org/10.1038/nature08460.

41. Orre, L.M., Vesterlund, M., Pan, Y., Arslan, T., Zhu, Y., Fernandez Woodbridge, A., Frings, O., Fredlund, E., and Lehtiö, J. (2019). SubCellBarCode: proteome-wide mapping of protein localization and relocalization. Mol. Cell *73*, 166–182.e7. https://doi.org/10.1016/j.molcel.2018.11.035.
42. Schwenk, J.M., Omenn, G.S., Sun, Z., Campbell, D.S., Baker, M.S., Overall, C.M., Aebersold, R., Moritz, R.L., and Deutsch, E.W. (2017). The Human Plasma Proteome Draft of 2017: building on the human plasma peptideAtlas from mass spectrometry and complementary assays. J. Proteome Res. *16*, 4299–4310. https://doi.org/10.1021/acs.jproteome.7b00467.
43. Viklund, H., Bernsel, A., Skwark, M., and Elofsson, A. (2008). SPOCTOPUS: a combined predictor of signal peptides and membrane protein topology. Bioinformatics *24*, 2928–2929. https://doi.org/10.1093/bioinformatics/btn550.
44. Uhlén, M., Fagerberg, L., Hallström, B.M., Lindskog, C., Oksvold, P., Mardinoglu, A., Sivertsson, Å., Kampf, C., Sjöstedt, E., Asplund, A., et al. (2015). Proteomics. Tissue-based map of the human proteome. Science *347*, 1260419. https://doi.org/10.1126/science.1260419.
45. Carroll, J.S., Meyer, C.A., Song, J., Li, W., Geistlinger, T.R., Eeckhoute, J., Brodsky, A.S., Keeton, E.K., Fertuck, K.C., Hall, G.F., et al. (2006). Genome-wide analysis of estrogen receptor binding sites. Nat. Genet. *38*, 1289–1297. https://doi.org/10.1038/ng1901.
46. Cohen, O., Mao, P., Nayar, U., Buendia-Bue, J.E., Kim, D., Jain, E., Helvie, K., Abravanel, D., Kowalski, K.J., Kapstad, C., et al. (2020). Acquired activating mutations in RTKs confer endocrine resistance in ER+ metastatic breast cancer through ER-reprogramming, MAPK signaling, and an induced stem-like cell state [abstract]. Cancer Res. In Proceedings of the 2019 San Antonio Breast Cancer Symposium. Abstract nr GS2-02.
47. Malorni, L., Giuliano, M., Migliaccio, I., Wang, T., Creighton, C.J., Lupien, M., Fu, X., Hilsenbeck, S.G., Healy, N., De Angelis, C., et al. (2016). Blockade of AP-1 potentiates endocrine therapy and overcomes resistance. Mol. Cancer Res. *14*, 470–481. https://doi.org/10.1158/1541-7786.MCR-15-0423.
48. Bi, M., Zhang, Z., Jiang, Y.Z., Xue, P., Wang, H., Lai, Z., Fu, X., De Angelis, C., Gong, Y., Gao, Z., et al. (2020). Enhancer reprogramming driven by high-order assemblies of transcription factors promotes phenotypic plasticity and breast cancer endocrine resistance. Nat. Cell Biol. *22*, 701–715. https://doi.org/10.1038/s41556-020-0514-z.
49. Creighton, C.J., Massarweh, S., Huang, S., Tsimelzon, A., Hilsenbeck, S.G., Osborne, C.K., Shou, J., Malorni, L., and Schiff, R. (2008). Development of resistance to targeted therapies transforms the clinically associated molecular profile subtype of breast tumor xenografts. Cancer Res. *68*, 7493–7501. https://doi.org/10.1158/0008-5472.CAN-08-1404.
50. Rueda, O.M., Sammut, S.J., Seoane, J.A., Chin, S.F., Caswell-Jin, J.L., Callari, M., Batra, R., Pereira, B., Bruna, A., Ali, H.R., et al. (2019). Dynamics of breast-cancer relapse reveal late-recurring ER-positive genomic subgroups. Nature *567*, 399–404. https://doi.org/10.1038/s41586-019-1007-8.
51. Curtis, C., Shah, S.P., Chin, S.F., Turashvili, G., Rueda, O.M., Dunning, M.J., Speed, D., Lynch, A.G., Samarajiwa, S., Yuan, Y., et al. (2012). The genomic and transcriptomic architecture of 2,000 breast tumours reveals novel subgroups. Nature *486*, 346–352. https://doi.org/10.1038/nature10983.
52. Győrffy, B. (2021). Survival analysis across the entire transcriptome identifies biomarkers with the highest prognostic power in breast cancer. Comput. Struct. Biotechnol. J. *19*, 4101–4109. https://doi.org/10.1016/j.csbj.2021.07.014.
53. Ciriello, G., Gatza, M.L., Beck, A.H., Wilkerson, M.D., Rhie, S.K., Pastore, A., Zhang, H., McLellan, M., Yau, C., Kandoth, C., et al. (2015). Comprehensive molecular portraits of invasive lobular breast cancer. Cell *163*, 506–519. https://doi.org/10.1016/j.cell.2015.09.033.
54. Jeselsohn, R., Buchwalter, G., De Angelis, C., Brown, M., and Schiff, R. (2015). ESR1 mutations-a mechanism for acquired endocrine resistance in breast cancer. Nat. Rev. Clin. Oncol. *12*, 573–583. https://doi.org/10.1038/nrclinonc.2015.117.
55. Jeselsohn, R., Bergholz, J.S., Pun, M., Cornwell, M., Liu, W., Nardone, A., Xiao, T., Li, W., Qiu, X., Buchwalter, G., et al. (2018). Allele-specific chromatin recruitment and therapeutic vulnerabilities of ESR1 activating mutations. Cancer Cell *33*, 173–186.e5. https://doi.org/10.1016/j.ccell.2018.01.004.
56. Gu, G., Tian, L., Herzog, S.K., Rechoum, Y., Gelsomino, L., Gao, M., Du, L., Kim, J.A., Dustin, D., Lo, H.C., et al. (2021). Hormonal modulation of ESR1 mutant metastasis. Oncogene *40*, 997–1011. https://doi.org/10.1038/s41388-020-01563-x.
57. Chandarlapaty, S., Chen, D., He, W., Sung, P., Samoila, A., You, D., Bhatt, T., Patel, P., Voi, M., Gnant, M., et al. (2016). Prevalence of ESR1 mutations in cell-free DNA and outcomes in metastatic breast cancer: a secondary analysis of the BOLERO-2 clinical trial. JAMA Oncol. *2*, 1310–1315. https://doi.org/10.1001/jamaoncol.2016.1279.
58. Stender, J.D., Nwachukwu, J.C., Kastrati, I., Kim, Y., Strid, T., Yakir, M., Srinivasan, S., Nowak, J., Izard, T., Rangarajan, E.S., et al. (2017). Structural and molecular mechanisms of cytokine-mediated endocrine resistance in human breast cancer cells. Mol. Cell *65*, 1122–1135.e5. https://doi.org/10.1016/j.molcel.2017.02.008.
59. Theodorou, V., Stark, R., Menon, S., and Carroll, J.S. (2013). GATA3 acts upstream of FOXA1 in mediating ESR1 binding by shaping enhancer accessibility. Genome Res. *23*, 12–22. https://doi.org/10.1101/gr.139469.112.
60. Eeckhoute, J., Keeton, E.K., Lupien, M., Krum, S.A., Carroll, J.S., and Brown, M. (2007). Positive cross-regulatory loop ties GATA-3 to estrogen receptor alpha expression in breast cancer. Cancer Res. *67*, 6477–6483. https://doi.org/10.1158/0008-5472.CAN-07-0746.
61. Jozwik, K.M., and Carroll, J.S. (2012). Pioneer factors in hormone-dependent cancers. Nat. Rev. Cancer *12*, 381–385. https://doi.org/10.1038/nrc3263.
62. Lambert, A.W., Pattabiraman, D.R., and Weinberg, R.A. (2017). Emerging biological principles of metastasis. Cell *168*, 670–691. https://doi.org/10.1016/j.cell.2016.11.037.
63. Obenauf, A.C., Zou, Y., Ji, A.L., Vanharanta, S., Shu, W., Shi, H., Kong, X., Bosenberg, M.C., Wiesner, T., Rosen, N., et al. (2015). Therapy-induced tumour secretomes promote resistance and tumour progression. Nature *520*, 368–372. https://doi.org/10.1038/nature14336.
64. Gao, N., Le Lay, J., Qin, W., Doliba, N., Schug, J., Fox, A.J., Smirnova, O., Matschinsky, F.M., and Kaestner, K.H. (2010). Foxa1 and Foxa2 maintain the metabolic and secretory features of the mature beta-cell. Mol. Endocrinol. *24*, 1594–1604. https://doi.org/10.1210/me.2009-0513.
65. Ye, D.Z., and Kaestner, K.H. (2009). Foxa1 and Foxa2 control the differentiation of goblet and enteroendocrine L- and D-cells in mice. Gastroenterology *137*, 2052–2062. https://doi.org/10.1053/j.gastro.2009.08.059.
66. Chen, P.S., Wang, M.Y., Wu, S.N., Su, J.L., Hong, C.C., Chuang, S.E., Chen, M.W., Hua, K.T., Wu, Y.L., Cha, S.T., et al. (2007). CTGF enhances the motility of breast cancer cells via an integrin-alphavbeta3-ERK1/2-dependent S100A4-upregulated pathway. J. Cell Sci. *120*, 2053–2065. https://doi.org/10.1242/jcs.03460.
67. Hsu, Y.L., Hung, J.Y., Liang, Y.Y., Lin, Y.S., Tsai, M.J., Chou, S.H., Lu, C.Y., and Kuo, P.L. (2015). S100P interacts with integrin alpha7 and increases cancer cell migration and invasion in lung cancer. Oncotarget *6*, 29585–29598. https://doi.org/10.18632/oncotarget.4987.
68. Patel, S., Ngounou Wetie, A.G., Darie, C.C., and Clarkson, B.D. (2014). Cancer secretomes and their place in supplementing other hallmarks of cancer. Adv. Exp. Med. Biol. *806*, 409–442. https://doi.org/10.1007/978-3-319-06068-2_20.
69. Yuen, K.C., Liu, L.F., Gupta, V., Madireddi, S., Keerthivasan, S., Li, C., Rishipathak, D., Williams, P., Kadel, E.E., 3rd, Koeppen, H., et al.

(2020). High systemic and tumor-associated IL-8 correlates with reduced clinical benefit of PD-L1 blockade. Nat. Med. *26*, 693–698. https://doi.org/10.1038/s41591-020-0860-1.

70. Schalper, K.A., Carleton, M., Zhou, M., Chen, T., Feng, Y., Huang, S.P., Walsh, A.M., Baxi, V., Pandya, D., Baradet, T., et al. (2020). Elevated serum interleukin-8 is associated with enhanced intratumor neutrophils and reduced clinical benefit of immune-checkpoint inhibitors. Nat. Med. *26*, 688–692. https://doi.org/10.1038/s41591-020-0856-x.
71. Peng, C., Chen, H., Wallwiener, M., Modugno, C., Cuk, K., Madhavan, D., Trumpp, A., Heil, J., Marmé, F., Nees, J., et al. (2016). Plasma S100P level as a novel prognostic marker of metastatic breast cancer. Breast Cancer Res. Treat. *157*, 329–338. https://doi.org/10.1007/s10549-016-3776-1.
72. Lukacik, P., Roversi, P., White, J., Esser, D., Smith, G.P., Billington, J., Williams, P.A., Rudd, P.M., Wormald, M.R., Harvey, D.J., et al. (2004). Complement regulation at the molecular level: the structure of decay-accelerating factor. Proc. Natl. Acad. Sci. USA *101*, 1279–1284. https://doi.org/10.1073/pnas.0307200101.
73. Liu, M., Yang, Y.J., Zheng, H., Zhong, X.R., Wang, Y., Wang, Z., Wang, Y.G., and Wang, Y.P. (2014). Membrane-bound complement regulatory proteins are prognostic factors of operable breast cancer treated with adjuvant trastuzumab: a retrospective study. Oncol. Rep. *32*, 2619–2627. https://doi.org/10.3892/or.2014.3496.
74. Mamidi, S., Cinci, M., Hasmann, M., Fehring, V., and Kirschfink, M. (2013). Lipoplex mediated silencing of membrane regulators (CD46, CD55 and CD59) enhances complement-dependent anti-tumor activity of trastuzumab and pertuzumab. Mol. Oncol. *7*, 580–594. https://doi.org/10.1016/j.molonc.2013.02.011.
75. De Angelis, C., Fu, X., Cataldo, M.L., Nardone, A., Pereira, R., Veeraraghavan, J., Nanda, S., Qin, L., Sethunath, V., Wang, T., et al. (2021). Activation of the IFN signaling pathway is associated with resistance to CDK4/6 inhibitors and immune checkpoint activation in ER-positive breast cancer. Clin. Cancer Res. *27*, 4870–4882. https://doi.org/10.1158/1078-0432.CCR-19-4191.
76. Morrison, G., Fu, X., Shea, M., Nanda, S., Giuliano, M., Wang, T., Klinowska, T., Osborne, C.K., Rimawi, M.F., and Schiff, R. (2014). Therapeutic potential of the dual EGFR/HER2 inhibitor AZD8931 in circumventing endocrine resistance. Breast Cancer Res. Treat. *144*, 263–272. https://doi.org/10.1007/s10549-014-2878-x.
77. Neve, R.M., Chin, K., Fridlyand, J., Yeh, J., Baehner, F.L., Fevr, T., Clark, L., Bayani, N., Coppe, J.P., Tong, F., et al. (2006). A collection of breast cancer cell lines for the study of functionally distinct cancer subtypes. Cancer Cell *10*, 515–527. https://doi.org/10.1016/j.ccr.2006.10.008.
78. Harvey, J.M., Clark, G.M., Osborne, C.K., and Allred, D.C. (1999). Estrogen receptor status by immunohistochemistry is superior to the ligand-binding assay for predicting response to adjuvant endocrine therapy in breast cancer. J. Clin. Oncol. *17*, 1474–1481. https://doi.org/10.1200/JCO.1999.17.5.1474.
79. Schneider, C.A., Rasband, W.S., and Eliceiri, K.W. (2012). NIH Image to ImageJ: 25 years of image analysis. Nat. Methods *9*, 671–675. https://doi.org/10.1038/nmeth.2089.
80. Langmead, B., and Salzberg, S.L. (2012). Fast gapped-read alignment with Bowtie 2. Nat. Methods *9*, 357–359. https://doi.org/10.1038/nmeth.1923.
81. Li, H., Handsaker, B., Wysoker, A., Fennell, T., Ruan, J., Homer, N., Marth, G., Abecasis, G., and Durbin, R.; 1000 Genome Project Data Processing Subgroup (2009). The Sequence Alignment/Map format and SAMtools. Bioinformatics *25*, 2078–2079. https://doi.org/10.1093/bioinformatics/btp352.
82. Heinz, S., Benner, C., Spann, N., Bertolino, E., Lin, Y.C., Laslo, P., Cheng, J.X., Murre, C., Singh, H., and Glass, C.K. (2010). Simple combinations of lineage-determining transcription factors prime cis-regulatory elements required for macrophage and B cell identities. Mol. Cell *38*, 576–589. https://doi.org/10.1016/j.molcel.2010.05.004.
83. Ramírez, F., Ryan, D.P., Grüning, B., Bhardwaj, V., Kilpert, F., Richter, A.S., Heyne, S., Dündar, F., and Manke, T. (2016). deepTools2: a next generation web server for deep-sequencing data analysis. Nucleic Acids Res. *44*, W160–W165. https://doi.org/10.1093/nar/gkw257.
84. Meerbrey, K.L., Hu, G., Kessler, J.D., Roarty, K., Li, M.Z., Fang, J.E., Herschkowitz, J.I., Burrows, A.E., Ciccia, A., Sun, T., et al. (2011). The pINDUCER lentiviral toolkit for inducible RNA interference in vitro and in vivo. Proc. Natl. Acad. Sci. USA *108*, 3665–3670. https://doi.org/10.1073/pnas.1019736108.
85. Gou, X., Anurag, M., Lei, J.T., Kim, B.J., Singh, P., Seker, S., Fandino, D., Han, A., Rehman, S., Hu, J., et al. (2021). Transcriptional reprogramming differentiates active from inactive ESR1 fusions in endocrine therapy-refractory metastatic breast cancer. Cancer Res. *81*, 6259–6272. https://doi.org/10.1158/0008-5472.CAN-21-1256.
86. Quinlan, A.R., and Hall, I.M. (2010). BEDTools: a flexible suite of utilities for comparing genomic features. Bioinformatics *26*, 841–842. https://doi.org/10.1093/bioinformatics/btq033.
87. Carroll, T.S., Liang, Z., Salama, R., Stark, R., and de Santiago, I. (2014). Impact of artifact removal on ChIP quality metrics in ChIP-seq and ChIP-exo data. Front. Genet. *5*, 75. https://doi.org/10.3389/fgene.2014.00075.
88. Dobin, A., Davis, C.A., Schlesinger, F., Drenkow, J., Zaleski, C., Jha, S., Batut, P., Chaisson, M., and Gingeras, T.R. (2013). STAR: ultrafast universal RNA-seq aligner. Bioinformatics *29*, 15–21. https://doi.org/10.1093/bioinformatics/bts635.
89. Trapnell, C., Williams, B.A., Pertea, G., Mortazavi, A., Kwan, G., van Baren, M.J., Salzberg, S.L., Wold, B.J., and Pachter, L. (2010). Transcript assembly and quantification by RNA-Seq reveals unannotated transcripts and isoform switching during cell differentiation. Nat. Biotechnol. *28*, 511–515. https://doi.org/10.1038/nbt.1621.
90. Wang, L., Wang, S., and Li, W. (2012). RSeQC: quality control of RNA-seq experiments. Bioinformatics *28*, 2184–2185. https://doi.org/10.1093/bioinformatics/bts356.
91. Waks, A.G., Cohen, O., Kochupurakkal, B., Kim, D., Dunn, C.E., Buendia Buendia, J., Wander, S., Helvie, K., Lloyd, M.R., Marini, L., et al. (2020). Reversion and non-reversion mechanisms of resistance to PARP inhibitor or platinum chemotherapy in BRCA1/2-mutant metastatic breast cancer. Ann. Oncol. *31*, 590–598. https://doi.org/10.1016/j.annonc.2020.02.008.
92. Nayar, U., Cohen, O., Kapstad, C., Cuoco, M.S., Waks, A.G., Wander, S.A., Painter, C., Freeman, S., Persky, N.S., Marini, L., et al. (2019). Acquired HER2 mutations in ER(+) metastatic breast cancer confer resistance to estrogen receptor-directed therapies. Nat. Genet. *51*, 207–216. https://doi.org/10.1038/s41588-018-0287-5.
93. Mao, P., Cohen, O., Kowalski, K.J., Kusiel, J.G., Buendia-Buendia, J.E., Cuoco, M.S., Exman, P., Wander, S.A., Waks, A.G., Nayar, U., et al. (2020). Acquired FGFR and FGF alterations confer resistance to estrogen receptor (ER) targeted therapy in ER(+) metastatic breast cancer. Clin. Cancer Res. *26*, 5974–5989. https://doi.org/10.1158/1078-0432.CCR-19-3958.
94. Fornes, O., Castro-Mondragon, J.A., Khan, A., van der Lee, R., Zhang, X., Richmond, P.A., Modi, B.P., Correard, S., Gheorghe, M., Baranašić, D., et al. (2020). JASPAR 2020: update of the open-access database of transcription factor binding profiles. Nucleic Acids Res. *48*, D87–D92. https://doi.org/10.1093/nar/gkz1001.
95. Grant, C.E., Bailey, T.L., and Noble, W.S. (2011). FIMO: scanning for occurrences of a given motif. Bioinformatics *27*, 1017–1018. https://doi.org/10.1093/bioinformatics/btr064.
96. Korotkevich, G., Sukhov, V., and Sergushichev, A. (2019). Fast gene set enrichment analysis. Preprint at bioRxiv. https://doi.org/10.1101/060012.

97. Trapnell, C., Roberts, A., Goff, L., Pertea, G., Kim, D., Kelley, D.R., Pimentel, H., Salzberg, S.L., Rinn, J.L., and Pachter, L. (2012). Differential gene and transcript expression analysis of RNA-seq experiments with TopHat and Cufflinks. Nat. Protoc. *7*, 562–578. https://doi.org/10.1038/nprot.2012.016.

98. Subramanian, A., Tamayo, P., Mootha, V.K., Mukherjee, S., Ebert, B.L., Gillette, M.A., Paulovich, A., Pomeroy, S.L., Golub, T.R., Lander, E.S., and Mesirov, J.P. (2005). Gene set enrichment analysis: a knowledge-based approach for interpreting genome-wide expression profiles. Proc. Natl. Acad. Sci. USA *102*, 15545–15550. https://doi.org/10.1073/pnas.0506580102.

99. Reich, M., Liefeld, T., Gould, J., Lerner, J., Tamayo, P., and Mesirov, J.P. (2006). GenePattern 2.0. Nat. Genet. *38*, 500–501. https://doi.org/10.1038/ng0506-500.

100. Zhang, Y., Liu, T., Meyer, C.A., Eeckhoute, J., Johnson, D.S., Bernstein, B.E., Nusbaum, C., Myers, R.M., Brown, M., Li, W., and Liu, X.S. (2008). Model-based analysis of ChIP-Seq (MACS). Genome Biol. *9*, R137. https://doi.org/10.1186/gb-2008-9-9-r137.

101. Kent, W.J., Zweig, A.S., Barber, G., Hinrichs, A.S., and Karolchik, D. (2010). BigWig and BigBed: enabling browsing of large distributed datasets. Bioinformatics *26*, 2204–2207. https://doi.org/10.1093/bioinformatics/btq351.

STAR★METHODS

KEY RESOURCES TABLE

REAGENT or RESOURCE	SOURCE	IDENTIFIER
Antibodies		
Rabbit polyclonal anti-ERalpha	Santa Cruz Biotechnology	sc-543X; RRID:AB_631471
Mouse monoclonal anti Drosophila histone variant H2Av	Active Motif	Cat#61752; RRID: AB_2793757
Rabbit polyclonal anti FOXA1	Abcam	ab23738; RRID:AB_2104842
Rabbit polyclonal anti GFP	Molecular Probes, Invitrogen	Cat#A-11122; RRID:AB_221569
Mouse monoclonal anti ER	Leica Biosystems	Cat#NCL-L-ER-6F11; RRID:AB_563706
Mouse monoclonal anti PR	DAKO	Cat#M3568; RRID:AB_2252608
Rabbit polyclonal anti IL8	Serotec	Cat#AHP781B; RRID:AB_2126224
Mouse monoclonal anti ER	Invitrogen	Cat#MA5-13304; RRID:AB_11002193
Rabbit polyclonal anti PR	Santa Cruz Biotechnology	sc-7208; RRID:AB_2164331
Rabbit monoclonal anti β-actin	Cell Signaling Technology	Cat#4970; RRID:AB_2223172
Mouse monoclonal anti IL-8 neutralizing antibody	R&D Systems	Cat#MAB208-100; RRID:AB_2249110
Mouse monoclonal IgG isotype	R&D Systems	Cat#MAB002; RRID:AB_357344
Bacterial and virus strains		
One Shot™ Stbl3™ Chemically Competent E. coli	Invitrogen	Cat#C737303
Biological samples		
MCF7 xenograft tumors	This paper	N/A
Chemicals, peptides, and recombinant proteins		
Slow-release estrogen (E2) (0.36 mg/60 days) pellet	Innovative Research	SE-121
Tamoxifen (Tam, 30 mg/kg in corn oil)	Sigma-Aldrich	T9262
D-Luciferin	Gold Biotechnology, St. Louis, MO	LUCK-100
β-Estradiol	Sigma-Aldrich	E2758
4-OH-tamoxifen	Sigma-Aldrich	CAS: 68047-06-3
Fulvestrant	Sigma-Aldrich	CAS: 129453-61-8
Doxycycline hyclate	Sigma-Aldrich	CAS: 24390-14-5
Critical commercial assays		
ELISA anti-IL8 kit	Raybiotech	ELH-IL-8
ELISA anti-S100P kit	Raybiotech	ELH-S100P
ELISA anti-EDN1 kit	Raybiotech	ELH-EDN1
ELISA anti-ANG kit	Raybiotech	ELH-ANG
ELISA anti-GOLM1 kit	Raybiotech	ELH-GOLM1
RNeasy Mini Kit	Qiagen	Cat# 74104
TruSeq RNA Sample Preparation Kit	Illumina	Cat# RS-122-2001
TruSeq ChIP Sample Prep Kit	Illumina	IP-202-1012
Qubit dsDNA HS Assay Kit	Thermo Fisher Scientific	Cat# Q32851
KAPA Hyper Library Preparation Kit	Roche	Cat# 07962347001
Deposited data		
RNA-seq raw and analyzed data	This paper	GSE175401
ChIP-seq raw and analyzed data	This paper	GSE175418
MCF7/FOXA1 −/+Dox: FOXA1 ChIP-seq	Fu et al.[29]	GSE124654
MCF7-P/TamR: FOXA1 ChIP-seq	Fu et al.[20]	GSE75201

(*Continued on next page*)

Continued

REAGENT or RESOURCE	SOURCE	IDENTIFIER
MCF7-P/TamR: ER ChIP-seq	Jeselsohn et al.[12]	GSE86538
MCF7/T47D/ZR75-1 P/endocrine-resistant lines: RNA-seq	De Angelis et al.[75]	GSE150997
MCF7-P/TamR: cJun ChIP-seq	Biet al.[48]	GSE128445
ER + metastatic cohort: RNA-seq and whole-exome seq	dbGaP	https://www.ncbi.nlm.nih.gov/projects/gapprev/gap/cgi-bin/study.cgi?study_id=phs001285.v1.p1
METABRIC gene expression dataset	synapse.sagebase.org	ID: syn1757063
Experimental models: Cell lines		
Human: MCF7 cells	Marc Lippman (Georgetown University Medical Center)	N/A
Human: MCF7 tamoxifen-resistant cells	Morrison et al./Fu et al.[20,76]	N/A
Human: MCF7 estrogen deprivation-resistant cells	Morrison et al./Fu et al.[20,76]	N/A
Human: MCF7 fulvestrant-resistant cells	Nardone et al.[38]	N/A
Human: T47D cells	Morrison et al./Nardone et al.[38,76]	N/A
Human: T47D tamoxifen-resistant cells	Nardone et al.[38]	N/A
Human: T47D estrogen deprivation-resistant cells	Morrison et al./Nardone et al.[38,76]	N/A
Human: T47D fulvestrant-resistant cells	Nardone et al.[38]	N/A
Human: ZR75-1 cells	ATCC	CRL-1500; RRID:CVCL_0588
Human: ZR75-1 tamoxifen-resistant cells	Fu et al./De Angelis et al.[20,75]	N/A
Human: ZR75-1 estrogen deprivation-resistant cells	Fu et al./De Angelis et al.[20,75]	N/A
Human: ZR75-1 fulvestrant-resistant cells	De Angelis et al.[75]	N/A
Human: 600MPE cells	Joe Gray (Oregon Health and Science University)[77]	N/A
Human: 600MPE tamoxifen-resistant cells	Fu et al.[20]	N/A
Human: 600MPE estrogen deprivation-resistant cells	Fu et al.[20]	N/A
Human: luciferase/GFP-tagged MCF7 cells	This paper	N/A
Human: doxycycline-inducible YFP-tagged MCF7 cells	This paper	N/A
Human: doxycycline-inducible DN-cJun-overexpression MCF7-TamR (1m)	This paper	N/A
Human: doxycycline-inducible DN-cJun-overexpression MCF7-TamR (1c)	This paper	N/A
Human: doxycycline-inducible sh-cJun MCF7-TamR cells	Biet al.[48]	N/A
Human: doxycycline-inducible FOXA1-overexpression MCF7	Fu et al.[20]	N/A
Human: doxycycline-inducible FOXA1-overexpression T47D	This paper	N/A
Human: doxycycline-inducible FOXA1-overexpression ZR75-1	Fu et al.[20]	N/A
Human: doxycycline-inducible IL8-overexpression MCF7	Fu et al.[20]	N/A
Experimental models: Organisms/strains		
Mouse: female ovariectomized mice: Hsd:Athymic Nude-Foxn1nu	Envigo (Indianapolis, IN)	069 - US

(*Continued on next page*)

Continued

REAGENT or RESOURCE	SOURCE	IDENTIFIER
Oligonucleotides		
siRNA FOXA1_ #1	Invitrogen	HSS104880
siRNA FOXA1_ #2	Invitrogen	HSS179280
siRNA ER_ #1	Invitrogen	VHS40912
siRNA ER_ #2	Invitrogen	VHS40913
AllStars Neg. Control siRNA	Qiagen	Cat#1027281
Recombinant DNA		
pXP-FOXA1-geneticin (TetOn)	Fu et al.[20]	N/A
Dual-tag (luciferase and GFP) vector	This paper	N/A
pInducer-dominant-negative (DNeg) c-Jun (TetOn)	This paper	N/A
Software and algorithms		
IncuCyte live-cell analysis system	Essen BioScience	https://www.sartorius.com/en/applications/life-science-research/cell-analysis/live-cell-assays/
The IVIS® Spectrum *in vivo* imaging system	PerkinElmer	https://www.perkinelmer.com/product/ivis-instrument-spectrum-120v-andor-c-124262
Celigo Image Cytometer	Nexcelom Bioscience	https://www.nexcelom.com/nexcelom-products/cellometer-and-celigo-image-cytometers/
ChemiDoc Touch Imaging System	Bio-Rad	Cat# 1708370
Allred nuclear IHC staining scoring method	Harvey et al.[78]	N/A
ImageJ	Schneider et al.[79]	https://imagej.nih.gov/ij/
Bowtie2	Langmead and Salzberg[80]	http://bowtie-bio.sourceforge.net/bowtie2/index.shtml
Samtools	Li et al.[81]	http://samtools.sourceforge.net
HOMER v4.9.1	Heinz et al.[82]	http://homer.ucsd.edu/homer/
deepTools2	Ramirez et al.[83]	https://deeptools.readthedocs.io/en/develop/
R v4.0.0	The R Project for Statistical Computing	https://cran.r-project.org/bin/windows/base/old/4.0.0/
Other		
Diagenode's Bioruptor® Standard	Diagenode	https://www.diagenode.com/en/documents/bioruptor-standard-manual

RESOURCE AVAILABILITY

Lead contact

Further information and requests for resources and reagents should be directed to and will be fulfilled by the lead contact, Xiaoyong Fu (xiaoyonf@wecurecancer.org).

Materials availability

Plasmids and cell lines generated in this study are available upon request via a material transfer agreement (MTA).

Data and code availability

- RNA-seq and ChIP-seq data generated in this study have been deposited at GEO under accession number GSE175401 and GSE175418, and are publicly available as of the date of publication. Accession numbers of sequencing data that were previously generated by us were listed in key resources table. Microscopy data reported in this paper will be shared by the lead contact upon request.
- This paper does not report original code.
- Any additional information required to reanalyze the data reported in this paper is available from the lead contact upon request.

EXPERIMENTAL MODELS AND SUBJECT DETAILS

Cell culture

Human breast cancer (BC) cell lines MCF7, ZR75-1, and T47D were purchased from American Type Culture Collection (ATCC). 600MPE cell line was obtained from the laboratory of Joe Gray (Oregon Health and Science University). All the parental (P) cells were grown in full medium, comprised of RPMI/1640 medium supplemented with 10% fetal bovine serum (FBS) and 1% penicillin/streptomycin/glutamine (PSG) (GIBCO) (for MCF7, ZR75-1, and T47D), or DMEM/high-glucose medium supplemented with 10% FBS and 1% PSG (for 600MPE). EndoR cell models were established as described previously[20,38,76] and maintained in phenol red-free medium supplemented with 10% charcoal-stripped FBS and 1% PSG, without (for EDR) or with the addition of 100 nM 4-OH-tamoxifen (Sigma) or 100 nM fulvestrant (Sigma) for TamR or FulR cells, respectively. Dox-inducible FOXA1-overexpressing MCF7-P/FOXA1 cells were infected with lentivirus packaging a dual tag (luciferase and GFP) vector obtained from Xiang Zhang (Baylor College of Medicine), sorted by GFP, and maintained as described.[20] The yellow fluorescence protein (YFP) and dominant-negative (DNeg) c-Jun TAM67 sequences, as we used previously,[47] were cloned into the Dox-inducible lentiviral vector, which was used in virus packaging and infection into MCF7-P or TamR cells, respectively, as we described previously.[20,84] Two individual MCF7-TamR cell clones (1c and 1m) engineered with Dox-inducible DNeg c-Jun overexpression were selected and maintained in geneticin (100 μg/mL). Cells were grown at 37°C, under a humidified atmosphere, with 5% CO_2. Cells have been authenticated by short tandem repeats DNA profiling and are routinely tested for mycoplasma status using the MycoAlert Mycoplasma Detection Kit (Lonza). All cell lines used here were established from female subjects.

Xenograft mouse model

Four to five-week-old female ovariectomized athymic nude (*Foxn1*^{nu}/*Foxn1*^{nu}) mice were obtained from Envigo (Indianapolis, IN) and housed in the Baylor College of Medicine Transgenic Mouse Facility. Mice were group housed under a 12:12 light/dark cycle with access to food and water *ad libitum*. All procedures were performed in accordance with a Baylor College of Medicine Institutional Animal Care and Use Committee-approved protocol.

METHOD DETAILS

In vivo tumor growth and metastasis modeling

Prior to cell injection, female athymic Foxn1nu nude mice were anesthetized by isoflurane vaporizer, and a slow-release estrogen (E2) (0.36 mg/60 days) pellet was implanted subcutaneously on the dorsal side below the shoulder blades. Two days later, log phase MCF7-P/FOXA/luc_GFP cells (8×10^6) were injected (in a 1:4 mixture of serum-free medium and Matrigel) subcutaneously under the second nipple. Tumor diameters and mouse weights were measured twice weekly, and tumor volume (vol; mm^3) was calculated as vol (mm^3) = $(\text{width})^2 \times \text{length}/2$. When the tumor reached a size of approximately 200 mm^3, mice were randomized to six experimental treatment groups (n = 12/group) which included continuous treatment with E2, estrogen deprivation (ED) alone (by removing the E2 pellet), or estrogen deprivation (ED) plus tamoxifen treatment (Tam, 30 mg/kg in corn oil, s.c., 5 times weekly). Each group was subsequently subdivided to −/+Dox (200 μg/mL) added in drinking water to test Dox-induced ectopic FOXA1 overexpression (OE). In ED and Tam groups, if tumor volume reached >600 mm^3, bioluminescence imaging (BLI) was performed 15–20 min after intraperitoneal injection of 75 mg/kg D-Luciferin (Gold Biotechnology, St. Louis, MO) using an IVIS Spectrum *in vivo* imaging system (PerkinElmer, Waltham, MA). Following imaging, survival surgery was performed on anesthetized mice to remove the primary tumors. After the surgery, mice treated with ED or Tam continued with their respective treatments. All the mice after surgery were monitored daily for health status, and BLI was performed twice monthly to monitor metastatic onset/status. Mice were euthanized by cervical dislocation under anesthesia when either a relapsed tumor reached a size of 1,500 mm^3, signs of morbidity defined by the animal protocol were evident, or the end of the experiment was reached. A detailed necropsy was performed after euthanization, and BLI was performed on the harvested lymph nodes, lung, and liver. All these tissues were chopped both for snap-freezing and for fixation in 10% formalin. Paraffin-embedded tissues were sectioned and stained with hematoxylin & eosin, and with antibodies in immunohistochemistry.

ChIP-seq

Cells were seeded in a 15cm dish in regular growth medium with −/+Dox (1 μg/mL) and split for two generations for 5 days. When cells were in their logarithmic growth phase, and at approximately 95% confluence, they were cross-linked with 1% formaldehyde for 10 min at room temperature and quenched with 125 mM glycine solution for 5 min. Cells were then rinsed twice and collected by a rubber scraper in ice-cold PBS supplemented with 1 mM phenylmethylsulfonyl fluoride (PMSF), pelleted at 4°C, 4,000 rpm for 5 min, and snap-frozen in liquid nitrogen for storage at −80°C. Cell pellets were resuspended at 4°C in ice-cold Cell Lysis Buffer containing 5 mM PIPES(pH 8.0), 85 mM KCl, 1% NP-40, protease inhibitor (Roche), and 1 mM PMSF. Cells were homogenized using a glass Douncer on ice and pelleted at 4°C, 4,000 rpm for 5 min. The nuclei pellets were then resuspended in Nuclei Lysis Buffer containing 50 mM Tris-HCl (pH 8.0), 10 mM EDTA, plus 1% SDS supplemented with protease inhibitor and 1 mM PMSF, and were sonicated using the Diagenode Bioruptor Standard instrument at a high amplitude and 30 sec-on/off program at 4°C for 20 min. Sheared chromatin was cleared from precipitates by centrifuging at 20,000 rpm for 10 min and then diluted using Dilution Buffer containing 20 mM

Tris-HCl (pH 8.0), 150 mM NaCl, 1 mM EDTA, 1% Triton X-100, and 0.01% SDS, plus protease inhibitor and 1 mM PMSF. The diluted chromatin was cleared from background binding using 40 μL Protein A/G Plus agarose beads (Santa Cruz Biotechnology) at 4°C for 30 min, and then incubated with antibodies against ER (Santa Cruz Biotechnology, sc-543X) or FOXA1 (Abcam, ab23738) in a rotator at 4°C overnight. We added spike-in *Drosophila melanogaster* chromatin (Active Motif) along with the antibody against histone variant H2Av (Active Motif, # 61752) as a ChIP-seq data normalization method. After an additional 1 h incubation with Protein A/G Plus beads at 4°C, the immunoprecipitates were washed consecutively twice in each type of buffer including the Low-Salt Wash Buffer containing 20 mM Tris-HCl (pH 8.0), 150 mM NaCl, 2 mM EDTA, 1% Triton X-100, 0.1% SDS, and 1 mM PMSF; High-Salt Wash Buffer containing 20 mM Tris-HCl (pH 8.0), 500 mM NaCl, 2 mM EDTA, 1% Triton X-100, 0.1% SDS, and 1 mM PMSF; LiCl Wash Buffer containing 20 mM Tris-HCl (pH 8.0), 250 mM LiCl, 1 mM EDTA, 1% NP-40, 1% Na-deoxycholate, and 1 mM PMSF; and TE buffer containing 10 mM Tris-HCl (pH 8.0), 1 mM EDTA, and 1 mM PMSF. Following washes, precipitates were eluted in Elution Buffer (50 mM NaHCO3 and 1% SDS) at 45°C and then supplemented with 300 mM NaCl. Crosslink reversal, including the 2.5% of chromatin input before ChIP, was done at 67°C for 12 h. ChIP DNA isolation was performed by RNA clearance using 0.2 mg/mL RNaseA at 37°C for 1.5 h, and then using a PCR purification kit (Qiagen). DNA concentration was measured using the Quant-iT PicoGreen dsDNA Assay Kit (Thermo Fisher Scientific).

Indexed libraries were prepared from ChIP DNA using the KAPA Hyper Library Preparation Kit (Kapa Biosystems). Libraries were amplified by 12 cycles of PCR, and then assessed for size distribution using the 4200 TapeStation High Sensitivity D1000 ScreenTape (Agilent Technologies), and quantified using the Qubit dsDNA HS Assay Kit (Thermo Fisher Scientific). The indexed libraries were multiplexed, 10 libraries per pool. The pool was quantified by qPCR using the KAPA Library Quantification Kit (KAPA Biosystems) and afterward sequenced on the Illumina NextSeq500 using the high-output 75-bp single-read configuration.

RNA-seq

Total RNA was extracted using the RNeasy Mini Kit (Qiagen). RNA was treated on columns with DNase I (Qiagen) prior to elution to remove DNA contamination. RNA-seq of the metastatic biopsies of ER + lesions from patients was guided by the Dana-Farber/Harvard Cancer Center Institutional Review Board protocol (DF/HCC 05–246). These samples were de-identified prior to use in this study. RNA-seq libraries were prepared using the TruSeq RNA Sample Preparation Kit (Illumina) adapted for use on the Sciclone (PerkinElmer) liquid handler, and sequenced on the Illumina NextSeq500 with single-end 75 bp reads. For samples from the MCF7-P cells treated with E2 or Tam and BC cells with ectopic H-FOXA1 OE, the RNA-seq libraries were prepared using the TruSeq RNA Sample Preparation Kit (Illumina) and sequenced on the Illumina HiSeq or Illumina NovaSeq6000, respectively, with paired-end 100 bp reads.

Immunohistochemistry

Immunohistochemistry was performed as described previously.[20] Briefly, freshly cut 3-μm sections from paraffin-embedded tissue blocks were deparaffinized and subjected to epitope retrieval in boiling citrate buffer (pH 6.0) or Tris buffer (pH 9.0) for 20 min. After blocking in 3% (v/v) hydrogen peroxide for 5 min, slides were incubated with normal IgG control (Santa Cruz Biotechnology), or antibody against GFP (1:500; A-11122, Molecular Probes, Invitrogen), FOXA1 (1:400; #ab23738, Abcam), ER (1:200; #NCL-L-ER-6F11, Leica Biosystems), PR (1:1,600; #M3568, DAKO), or IL-8 (1:500; #AHP781B, Serotec), all incubated at room temperature for 1 h, except for GFP, which was incubated at 4°C overnight. Immunodetection was performed with either the EnVision+ System (DakoCytomation), or the M.O.M. (Mouse on Mouse) Immunodetection Kit (Vector Laboratories) for GFP. The stained slides were independently reviewed by two researchers. The nuclear FOXA1 and paranuclear IL-8 staining was assessed using an Allred scoring method.[78]

Western blotting

Cells were seeded in 6-well plates in culture media described above. After 2 days when cells were still in their logarithmic growth phase and at 95% confluence, cells were washed in ice-cold PBS twice and lysed in RIPA Buffer containing 150 mM NaCl, 10 mM Tris-HCl (pH 7.2), 0.1% SDS, 1% Triton X-100, 1% sodium deoxycholate, and 5 mM EDTA, supplemented with protease inhibitor cocktail (Roche) and PhosSTOP phosphatase inhibitor cocktail (Roche) by rotating at 4°C for 15 min. Protein concentration was measured using the Pierce BCA Protein Assay Kit (Thermo Fisher Scientific) according to the manufacturer's instructions. Equivalent amounts of protein (20–25 μg) from each sample were resolved by NuPAGE 10% Bis-Tris gels (Life Technologies) and transferred using the iBlot2 Dry Blotting System (Life Technologies) onto nitrocellulose membranes. The membranes were first stained with Ponceau S (Thermo Fisher Scientific) to confirm uniform loading and transfer, and then blocked with 3% non-fat milk powder (Santa Cruz Biotechnology) at room temperature for 1 h, and incubated overnight at 4°C in PBST buffer (1× PBS, 5% BSA, 0.05% Tween 20) with primary antibodies against FOXA1 (1:1,000; #ab23738, Abcam), ER (1: 1,000; #MA5-13304, Invitrogen), PR (1:200; #sc-7208, Santa Cruz Biotechnology), or β-actin (1:2,000; #4970, Cell Signaling Technology). After washes with the PBST buffer, the membranes were incubated for an additional 1 h at room temperature with the appropriate horseradish peroxidase (HRP)-linked secondary antibodies (Cell Signaling Technology). Immunoblots were developed by the Amersham ECL Prime Detection Reagent (GE Healthcare) and scanned by the ChemiDoc Touch Imaging System (Bio-Rad). Densitometry analysis of the blots was performed using ImageJ 1.52q.[79]

Preparation of conditioned medium

The conditioned media (CM) were collected from MCF7-P, MCF7-TamR, and MCF7-P cells with Dox-inducible YFP (used as a negative control), FOXA1, or IL-8 OE. Briefly, MCF7-P and TamR cells were cultured for 48 h before being subjected to RPMI/1640 phenol red-free medium, supplemented with 10% charcoal-stripped FBS and with E2 (1 nM, for P cells) or 4-OH-tamoxifen (100 nM, for P and TamR cells), for an additional 24 h. The MCF7-P cells engineered with controllable gene OE were cultured under −/+ Dox (1 μg/mL) for 72 h before being subjected to replenished media for an additional 24 h. CM were collected after 24 h incubation and centrifuged, aliquoted, and stored at −80°C for later ELISA and migration assays. Before collecting CM, we used the imaging-based cytometer (Celigo, Nexcelom) to count cell number, which was used for the normalization in the following ELISA and migration assays.

ELISA

The secretion levels of 5 secretome factors (IL-8, S100P, GOLM1, EDN1, and ANG) were measured with a human ELISA kit (Raybiotech) according to the manufacturer's instructions. Briefly, the ELISA microplate precoated with antibody against secretome factors was incubated with CM collected from cells and the standard samples at room temperature for 2.5 h. The wells were washed three times with washing buffer and then incubated with the biotinylated antibody for 1 h. After removal of unbound biotinylated antibody with washing buffer, the wells were incubated with HRP-conjugated streptavidin for 45 min, followed by the addition of the substrate solution for additional 30 min of incubation. The reaction was then stopped by addition of the stop solution and the absorbance values were measured at 450 nm on a microplate reader (Thermo Scientific). The concentration of secretome factors in CM was calculated based on the standard curve and normalized by the number of cells giving rise to the CM.

Migration assay

For assays using CM, MCF7-P cells were seeded at 30,000–35,000 cells/well into a 96-well ImageLock plate (Essen BioScience) 24 h before treatment with 50 ng/mL mitomycin C (Sigma) for 2 h to inhibit proliferation. Cells were scratched with a WoundMaker (Essen BioScience), washed once with fresh media, and then cultured in CM collected from MCF7-P cells −/+Dox with ectopic OE of YFP or IL-8. For assays using neutralizing antibody, the wounded MCF7-P and TamR cells were incubated with media containing mitomycin C along with the IL-8 neutralizing antibody (2 μg/mL) (MAB208–100, R&D Systems) or IgG isotype control (MAB002, R&D Systems). Images were obtained with the IncuCyte live-cell analysis system (Essen BioScience) every 4 h for up to 72 h, during which the media including mitomycin C −/+ neutralizing antibody were changed every 24 h. The capacity of cell migration was assessed by calculation of the ratio of wound density within vs. outside of the wound area, as previously described.[85] For assays using CM, the relative wound density was further normalized by the number of cells giving rise to the CM.

ChIP-seq data analysis

Reads from ChIP-seq experiments were mapped to the reference genomes of human (hg19) and *Drosophila melanogaster* (dm3) using Bowtie 2 v2.3.4.1.[80] Uniquely mapped reads with no more than two mismatches were retained for further analysis. Samtools v1.10[81] was used to index the BAM files and get the read count (RC). The scaling factor was calculated for each BAM file in the same target ChIP-seq experiments using the formula: $(RC_{target}/RC_{spike\text{-}in})/[RC_{target}/RC_{spike\text{-}in}]_{max}$. The BAM files were then downsampled using Picard v2.17.8 (http://broadinstitute.github.io/picard/) for ChIP-seq spike-in normalization.

We used the getDifferentialPeaksReplicates.pl command line in HOMER v4.9.1[82] with the arguments of "-fdr 0.001 -F 2 -L 2 -f 2 -q 0.05" to call the FOXA1 peaks against the input DNA as a background control. As ER ChIP-seq in cells grown in full medium without estrogen supplementation yielded a smaller number of peaks, we used a lesser stringent setting of "-fdr 0.05 -F 2 -L 2 -f 2 -q 0.1" in the command line for peak calling. The differential peaks (gain, share, and loss) between samples in comparison were obtained using the bedtools v2.29.2.[86] The ChIP-seq overall quality was assessed using ChIPQC v1.30.0.[87]

Genome signal tracks of TF binding were generated using the bamCoverage command line in deepTools2[83] by converting the downsampled BAM files to a bigWig format with a fixed bin size of 10 bp. To produce the heatmaps, we generated a score matrix of genomic coverage centered at the peak summit with ±2 kb flanking regions in 50 bp bins, and visualized the matrix in scaled colors and in a descending order within clustered peak regions, using the computeMatrix and plotHeatmap command lines in deepTools2,[83] respectively. All metaplots of binding signals were produced by computing the average coverage scores for each 50 bp bin within ±500 bp or 2 kb from the peak summit in the given set of genomic regions.

RNA-seq and microarray data analysis

Reads were mapped to the human genome (hg19) using STAR v2.5.1[88] followed by transcript assembly using cufflinks v2.2.1.[89] RNA-seq quality control was done using RseQC v2.6.2.[90] Relative transcript abundance (RPKM) was calculated using Cufflinks v2.2.1.[89] Prior to log2 transformation of RPKM values, a pseudo-count of 1 was added to all RPKM values. RNA-seq of the metastatic biopsies of ER + lesions from patients was analyzed as described previously.[91] The *FOXA1* amplification status and *FOXA1/ESR1* mutational status of the metastatic ER + cohort were obtained from the whole exome-seq as described previously.[92,93]

We retrieved our published microarray dataset for the MCF7 xenograft tumors.[49] We performed differential gene expression (DGE) analysis using data from the E2/Tam-treated MCF7-P cells, MCF7-TamR cells upon ER/FOXA1 KD and MCF7-P cells upon FOXA1 OE, as we previously reported,[20] and from the MCF7-TamR cells with Dox-inducible c-Jun KD. We used the gene count matrix data (GSE128460)[48] obtained in MCF7-TamR cells upon c-Jun KD to perform DGE analysis using the limma R package (3.46.0). The

METABRIC gene expression dataset[51] was downloaded from Synapse (synapse.sagebase.org) via authorized access. Expression of a gene represented multiple times in METABRIC and in the gene expression mega-set KM-plotter[52] on a given platform was determined by selecting the probe with the greatest variation across samples. Expression levels of the target genes were compared among tumors grouped by pathological ER/PR/HER2 status annotated in the METABRIC molecular dataset.[50]

Motif enrichment analysis

For motif discovery, the findMotifsGenome.pl command line in HOMER v4.9.1[82] was used to search the regions with 200 bp upstream and downstream of the peak summit, based on the cumulative hypergeometric distribution model with random matched genomic control regions used as background sequence.

Genomic motif scanning and positional gene expression analysis

For motif scanning analysis, we first generated a fasta file representing all genomic enhancer regions in MCF7-P/FOXA1 −/+Dox cells by merging the regions marked with H3K27ac and H3K4me1 (data from GSE124654[29]). We then used an eleven position-weight matrix (from JASPAR: MA0148.1)[94] to map the FOXA1 motif reservoir across these enhancer regions using FIMO v4.11.2[95] with an assignment significance of $p < 1 \times 10^{-4}$. To correlate the number of FOXA1-bound FOXA1 motif and gene expression, we first determined the genes harboring the FOXA1-bound FOXA1 motif within ±250 kb from the transcription start site (TSS), and then stratified the genes based on the net FOXA1 motif change between MCF7-P/FOXA1 +Dox vs. -Dox cells.

Binding and Expression Target Analysis (BETA)

To infer TF direct target genes, we correlated the TF-bound peaks identified by ChIP-seq and the TF perturbation-induced differentially expressed genes determined by RNA-seq using BETA v1.0.7.[33] The direct UP and DN target genes were selected from the BETA output gene lists using the cutoff of rank product (p value) < 0.01 and expressional $\log_2$(fold change) > 1 and < −1, respectively.

Ontology annotation, gene set enrichment analysis (GSEA), and single-sample (ss) GSEA

Functional annotation of target gene sets was done by Gene Ontology (GO) analysis using DAVID v6.8.[36] The top 11 GO terms enriched in the Biological Process database were plotted in bar charts indicating both the number of overlapping genes and the transformed p value calculated by DAVID modified Fisher's exact test.

GSEA of target gene sets in a preranked gene list was performed using an algorithm of adaptive multilevel split Monte Carlo implemented in fgsea v 3.11.[96] Preranked gene lists were generated by sorting the differentially expressed genes between two conditions in RNA-seq using the statistic t value calculated by Cuffdiff.[97] To evaluate the significance of FOXA1-CGS in comparison to other pathways, we performed GSEA using a custom set of pathways including the 50 hallmark gene sets from MSigDB v6.2.[98] The normalized enrichment score (ES) and transformed adjusted p value were presented using volcano plots.

For ssGSEA, the target gene sets and GCT file generated from the RNA-seq data were loaded into the ssGSEA v10.0.1 module[40] in GenePattern v 3.9.11.[99] The analysis was run using the default settings with the combine.add mode to calculate a combined ES for UP and DN gene sets for each sample. The output values of ES were normalized by z-transformation and used to evaluate the activation status of the target pathway across variant cell models.

Unsupervised hierarchical clustering

Hierarchical cluster analysis was performed using the hclust function in the R Stats v3.6.2 package. The clustering was run using the z-transformed gene expression data by the complete linkage method based on the similarities calculated by (1 – correlation coefficient) among genes and samples. The results of clustering were visualized in heat maps using the R pheatmap v1.0.12 package, with the dendrogram trees cut by k = 2 to differentiate the clusters of the FOXA1-CGS UP/DN gene sets and the cell models.

Secretome enrichment analysis

The FOXA1-CGS UP/DN genes were assigned to five groups encoding proteins distributed across different subcellular compartments of MCF7 cells.[41] The compartment enrichment analysis was performed using the chi-square test with the Bonferroni multicomparison adjustment, with the expressional no-change genes predicted by BETA (n = 1,093) as the control gene set.

Calculation of average modified *Z* score (AveMZ)

We used the modified Z score to transform the gene expression data because it relies on the median and is less influenced by outliers when compared to the standard Z score based on the mean. The score was calculated by the formula of (X-MED)/(1.486*MAD), where X is the log-transformed gene expression value (e.g., $\log_2$(1+RPKM) for RNA-seq data), MED is the median level of X across samples, and MAD (≠ 0) is the median absolute deviation calculated by MAD = median(|X - median(X)|). The signature score of the target gene set was presented as AveMZ by calculating the mean of modified Z-scores of the signature genes for individual samples.

METABRIC and KM-plotter data analyses

Breast tumor gene expression profiles with clinicopathologic data were obtained from METABRIC[50,51] via authorized access in Synapse (synapse.sagebase.org) and from a mega-set KM-plotter.[52] Kaplan-Meier plots were produced using the R survminer v0.4.8

package to display the survival probabilities per group as a function of time. Groups of ER + BC cohorts were stratified by the median or top-tertile cutoff of single gene expression or gene signature score. Hazard ratio (HR) of stratum and *p* value were calculated using the Wald estimates and likelihood ratio test, respectively, in the Cox proportional hazards model using the R survival v3.2-3 package.

A multivariate Cox proportional hazards model was computed using the R survival v3.2-3 package to assess simultaneously the effect of clinicopathologic factors (e.g., tumor size, stage, and LN status) and the expression of target genes on specified patient outcomes within a fixed time frame (5 or 15 yrs) of follow-up. The forest plots were used to display the HR with 95% confidence intervals for each factor included in the multivariate analysis, with $p < 0.05$ considered statistically significant.

Target gene set *cis*-regulatory TF binding analysis

To compare the intensity of TF binding at genomic regions of a target gene set across samples, we used a customized analytic approach comprising (*i*) call peaks using MACS2 v2.1.0[100] with a bandwidth parameter of 150 bp; (*ii*) make a union of peaks identified in all samples; (*iii*) scale BAM files across samples and convert the scaled BAM to a tag directory using the makeTagDirectory command line in HOMER v4.9.1;[82] (*iv*) convert bedGraph files in tag directories to a bigWig format using kentutils v302.1;[101] (*v*) assign union peaks to the nearest TSS using the annotatePeaks.pl command line in HOMER v4.9.1[82] and subtract the peaks that are located within 2 kb (for promoters) or 2–100 kb (for enhancers) of TSS of target genes; (*vi*) calculate tag densities across bigWig score files over the subtracted peaks with ±2 kb flanking regions from peak summit in 50 bp bins, using deepTools2;[83] (*vii*) calculate tag densities across tag directories over the subtracted peaks using the annotatePeaks.pl command line with an argument "-d" in HOMER v4.9.1 8882; and (*viii*) aggregate tag densities per gene, calculate mean across grouped samples, and make heat maps using the R pheatmap v1.0.12 package.

QUANTIFICATION AND STATISTICAL ANALYSIS

Statistical analyses

All statistical analyses were performed using R v4.0.0. Quantitative data are presented as mean ± SEM from n samples as indicated. Groups of data points were compared using a paired or unpaired two-sample t test, a Welch's t test for samples with unequal variance, a non-parametric Wilcoxon rank-sum test, or a two-sided Kolmogorov-Smirnov test to compare empirical cumulative distributions of data points. Comparison among groups ($n \geq 3$) was performed using the one-way ANOVA test or the pairwise t test with multiple test corrections. For comparing distribution of target genes or TF binding peaks among different groups, statistical analyses were performed using the chi-square test with the Bonferroni multi-comparison adjustment. For tumor mRNA analyses, a Pearson or Spearman correlation coefficient test was performed to determine the correlation between expression levels of target genes or gene sets. For cell line experiments, biological duplicates were used for ChIP-seq and RNA-seq, and triplicates were used for immunoblotting. Where appropriate, $p < 0.05$ was considered statistically significant.